Report No. DOT-TST 76T-20

CONCRETE REINFORCED WITH PLAIN AND DEFORMED STEEL FIBERS

AUGUST 1976

FINAL REPORT

Prepared for

U.S. Department of Transportation
OFFICE OF THE SECRETARY
AND
FEDERAL RAILROAD ADMINISTRATION
Washington, D.C. 20590

NOTICE

This document is disseminated under the sponsorship of the Department of Transportation in the interest of information exchange. The United States Government assumes no liability for its contents or use thereof.

The United States Government and the University of Illinois at Urbana-Champaign do not endorse products or manufacturers. Trade or manufacturer's names appear herein solely because they are considered essential to the object of this report.

Technical Report Documentation Page

1. Report No.	2. Government Accession No.	3. Recipient's Catalog No.
DOT-TST 76T-20		

4. Title and Subtitle	5. Report Date
Concrete Reinforced with Plain and Deformed Steel Fibers	August 1976
	6. Performing Organization Code
	8. Performing Organization Report No.
7. Author's)	UILU-ENG-76-2011
Grant T. Halvorsen	
9. Performing Organization Name and Address	10. Work Unit No. (TRAIS)
Department of Civil Engineering University of Illinois at Urbana-Champaign Urbana, IL 61801	11. Contract or Grant No. DOT FR 30022
	13. Type of Report and Period Covered FINAL REPORT December 1974 to August 1976
12. Sponsoring Agency Name and Address Office of the Secretary and Federal Railroad Administration U.S. Department of Transportation Washington, D. C. 20590	14. Sponsoring Agency Code

15. Supplementary Notes

16. Abstract This study was undertaken to determine what benefits might result from using deformed steel fiber reinforcement in portland cement concrete.

The experimental investigation included two plain and four deformed fibers. Mixes were designed for fiber contents of 0.9 and 1.5 percent by volume. Plain concretes with similar workability were formulated for comparison. Compressive strength, modulus of rupture, direct tensile strength, and flexural load-deflection curves were determined from specimens of each mix design. The load-deflection curves were used to analytically determine moment-curvature and tensile stress-strain relationship.

Ultimate strength is generally insensitive to characteristics of fiber deformation. Significant differences in load-deflection behavior are evident, and apparently related to fiber material, deformation, and content.

This study suggests that with ductile fibers, the ultimate flexural load can exceed the cracking load if the product of the fiber content and the fiber aspect ratio ($\rho \cdot \ell/d$) exceeds a critical value. The critical value of this project for a ductile composite is tentatively 90 for straight fibers. The critical value is less for properly anchored fibers, but the exact value is uncertain. Influence of concrete matrix strength, relative size of fiber and member, and fiber orientation have not been considered.

With properly anchored fibrous reinforcement, the required fiber content to achieve specified properties can be reduced. A reduction in fiber content will permit a reduction of the paste content required for workability.

17. Key Words	18. Distribution Statement
Concrete; Fiber Reinforced Concrete; Mechanical Properties; Ductility	Document is available to the public through the National Technical Information Service, Springfield, VA 22151

19. Security Classif. (of this report)	20. Security Classif. (of this page)	21. No. of Pages	22. Price
Unclassified	Unclassified	71	

Form DOT F 1700.7 (8-72) Reproduction of completed page authorized

PREFACE

Research described in this report was performed in the Department of Civil Engineering, University of Illinois at Urbana-Champaign, during the period December 1974 to August 1976. The work is a result of the investigation of steel fiber reinforced concrete as a material for slipformed tunnel liners, and interest in designing the best concrete for this purpose. With the development of commercial deformed fibers, it became apparent that a comparison of the behavior of concretes reinforced with various types of steel fibers would be useful in evaluation of these new materials. These comparisons may be of specific interest in selecting mixes and equipment for concrete tunnel liners, and of general interest with respect to development of fibrous reinforcement with different anchorage characteristics.

This research was sponsored by the U.S. Department of Transportation through Contract No. FR 30022. Mr. Russell K. McFarland was the contracting officer's technical representative.

This report is based on a thesis submitted by the author in partial fulfillment of the requirements for the degree of Master of Science in Civil Engineering. The guidance and encouragement provided by Clyde E. Kesler, Professor of Civil Engineering and of Theoretical and Applied Mechanics, throughout the course of this investigation is gratefully acknowledged. The approach to the experimental and analytical procedures benefitted from discussions with A. R. Robinson, Professor of Civil Engineering, S. L. Paul, Assistant Professor of Civil Engineering, and fellow graduate students.

This investigation was aided by the interest of the Bekaert Steel Wire Corporation, and the U.S. Steel Corporation, who supplied deformed steel fibers which were commercially unavailable in the U.S.A.

TABLE OF CONTENTS

LIST OF FIGURES

LIST OF SYMBOLS

d = Fiber diameter, or diameter of a circle with equivalent cross section;

EI = Elastic stiffness of a cross section;

ℓ = Fiber length;

ℓ/d = Fiber aspect ratio;

M = Bending moment;

$\Delta M'$ = Change in slope of moment-curvature relationship at cracking;

f'_c = Compressive strength of 4 in. by 8-in. (100 mm by 200-mm) test cylinder;

f'_r = Modulus of rupture of 3 in. by 3 in. by 15-in. (75 mm by 75 mm by 380-mm) beam specimen in third-point loading;

f^*_r = Modulus of rupture of 4 in. by 6 in. by 64-in. (100 mm by 150 mm by 1625-mm) beam in sixth-point loading;

f'_t = Nominal gross tensile strength;

S = Elastic section modulus;

e = Fiber reinforcement content, expressed as a percentage of total volume;

σ_o = M/S, the linear flexural stress at cracking;

$\Delta\sigma$ = The tensile stress drop at cracking;

ϕ = Curvature, the second derivative of deflection with respect to length;

ϕ_1 = M/EI, the linear component of curvature; and

ϕ_2 = The assumed constant curvature in the vicinity of a flexural crack.

CHAPTER 1

INTRODUCTION AND SCOPE

1.1 INTRODUCTION

Fiber reinforced concrete has advanced from a material of academic interest to a material which can be utilized in the solution of significant engineering problems.

Suitability for a particular application is determined by the ultimate criteria of economic feasibility. In-place performance must be considered with respect to costs of material, handling, and placement. Any improvement in the technology of fiber reinforced concrete which results in improved performance at a specific fiber content will influence the overall applicability of the material. Such an improvement may relate to any of the cost items, material, handling, and placement, which increase the expense of a given fibrous concrete.

Concern for depleting resources and skyrocketing costs of construction materials and processes necessitates efficient utilization of raw materials.

When fibrous reinforcement is included in a concrete matrix, the primary benefit is derived from postcracking behavior. A particular strength can be obtained with plain concrete, but the material is brittle. Fibers will affect the material behavior after cracking, up to, and after the maximum load carrying capacity. In reference to the ultimate strength of fiber reinforced concrete, ACI Committee 544 [1]* observed ". . . the maximum load is controlled primarily by fibers gradually pulling out, and the stress in the fiber at the ultimate load is substantially less than the yield stress of the fiber".

*Numbers in brackets refer to the List of References.

There is obvious benefit in the mobilization of a significant proportion of individual fiber strength in the improvement of postcracking behavior, in terms of strength and toughness. To achieve this mobilization fiber pullout must be delayed either by improving bond at the fiber-matrix interface, or by the provision of mechanical interlocks. This latter mechanism is defined as anchorage and may be due either to deformations distributed over the length of the fiber or to a concentrated deformation at the end of the fiber.

The hypothesis of this investigation is that fiber anchorage is the dominant factor in determining postcracking behavior of fiber reinforced concrete. Consequently, similar overall behavior should be attainable at different reinforcement percentages for different fibers, depending on bond and anchorage characteristics.

1.2 PRIOR INVESTIGATIONS

Although most research to date in steel fiber reinforced concrete has been performed with round or flat rectangular fibers, both of which are commercially available and readily manufactured, work with other geometries has been reported.

Luke, Waterhouse and Wooldridge [13], Johnston [9], and Johnston and Coleman [10] have reported tests of round, flat and Duoform [16] fibers. The shaped Duoform fiber has alternating flat and round sections. Henry [7], and Burnett, Constable and Cover [4] have reported applications of the Duoform fiber to precast concrete products. Edgington, Hannant and Williams [6] tested round, Duoform, and crimped fibers. Batson, Jenkins and Spatney [3]

investigated specimens with round, flat, and crimped fibers. Taylor [19] tested specimens with closed loop reinforcement. Moens [14], and Dehousse and LeJeune [5] reported flexural tests of several deformed fibers: Duoform, crimped, and fibers with bends at either end.

The aforementioned investigations reported the performance of fibrous reinforcement within a concrete matrix in a loaded test specimen. Reinforcement quantities for such tests are not excessive in terms of weight, but can be prohibitive if fibers of a specified design must be fabricated. Some exotic geometries and surface treatments have been evaluated by means of pullout tests by Tattersall and Urbanowicz [18] and by Kesler [12]. Pullout loads for the fibers studied in this investigation are reported in Appendix A.

1.3 SCOPE

The investigation reported herein consists of an experimental and analytical study of the behavior in compression, tension and flexure of fibrous concretes cast with six types of steel fiber, each possessing unique anchorage characteristics. Particular attention is given to the postcracking behavior in flexure and tension. This emphasis reflects the observation that the most significant properties of fiber reinforced concrete are ductility and toughness. A particular strength may be obtained from plain concrete at a much lower cost. Two fiber contents, 0.9 and 1.5 volume percent, were tested for each type of fiber. Several plain concretes were tested for specific purposes of comparison with the fiber reinforced concrete mixes.

CHAPTER 2

EXPERIMENTAL MATERIALS AND METHODS

2.1 MATERIALS

2.1.1 AGGREGATE

The coarse aggregate used was nominal 3/8-in. (10-mm) maximum size Wabash River pea gravel. Fine aggregate was a locally available sand.

Gradations, unit weights, bulk specific gravities and absorption capacities for the sand and pea gravel are shown in Tables 2.1 and 2.2.

2.1.2 CEMENT AND FLY ASH

One lot of commercial portland cement, type 1, packaged in sacks, was used for all experimental work. One lot of ASTM C-618 Class F fly ash, packaged in sacks, was used as described in Section 2.2., Mix Design.

2.1.3 FIBROUS REINFORCEMENT

Six characteristic geometries of steel fiber reinforcement were investigated. Some are currently available for commercial application while others have been produced for purposes of research and development.

Significant characteristics of the fibers are summarized in Table 2.3; each fiber is pictured in Fig. 2.1.

2.2 MIX DESIGN

The mix designs for fiber reinforced concrete were obtained from ongoing research regarding pumpable concretes for application to tunnel

TABLE 2.1

SIEVE ANALYSIS OF SAND AND PEA GRAVEL

Sieve	Sand, percent		Pea gravel, percent	
	Retained	Passing	Retained	Passing
3/8-in. (10-mm)	0	100	1	99
No. 4 (4.75-mm)	4	96	94	6
No. 8 (2.36-mm)	12	88	99	1
No. 16 (1.18-mm)	22	78	100	0
No. 30 (600-μm)	40	60	100	0
No. 50 (300-μm)	84	16	100	0
No. 100 (150-μm)	99	1	100	0
No. 200 (75-μm)	99	1	100	0
Fineness Modulus	2.61		5.93	

TABLE 2.2

PROPERTIES OF SAND AND PEA GRAVEL

Property	Sand	Pea gravel
Unit weight, lb/cu ft (kg/m^3)	107.6 (1724)	100.6 (1612)
Bulk specific gravity, ssd	2.60	2.66
Absorption capacity, percent	2.2	2.2

TABLE 2.3

PROPERTIES OF FIBROUS REINFORCEMENT

Type	Cross section	Length, in. (mm)	$\frac{\ell}{d}$	Geometry
F	0.010 in. by 0.022 in. (0.25 mm by 0.56 mm)	1 (25)	60	Straight
I	0.010 in. by 0.022 in. (0.25 mm by 0.56 mm)	1 (25)	60	Enlarged ends 0.032 in. by 0.045 in. (0.81 mm by 1.14 mm)
H	Irregular 0.02-in. equivalent dia. (0.51-mm)	1.4 (35)	70	Irregular, made from hot melt
R	0.016-in. dia. (0.41-mm)	1 (25)	63	Straight, brass coated
W	0.017-in. dia. (0.43-mm)	1 (25)	59	Seven waves, made crimping
B	0.016-in. dia. (0.40-mm)	1.7 (43)	108	Two 65-deg bends at each end

liners. Pumpable concrete requires minimum void volume, which is accomplished by proper aggregate size and gradation, and paste content. Fly ash is used as a cement replacement, and as a means of providing additional fines required for workability. The laboratory investigations regarding pumpable concrete have been reported by Ounanian, Halvorsen, and Kesler [15]. Kesler [11] has reported the influence of fly ash on the properties of steel fiber reinforced concrete.

Fiber contents of 0.9 and 1.5 volume percent were chosen from previous experience with the properties of fresh and hardened steel fiber reinforced

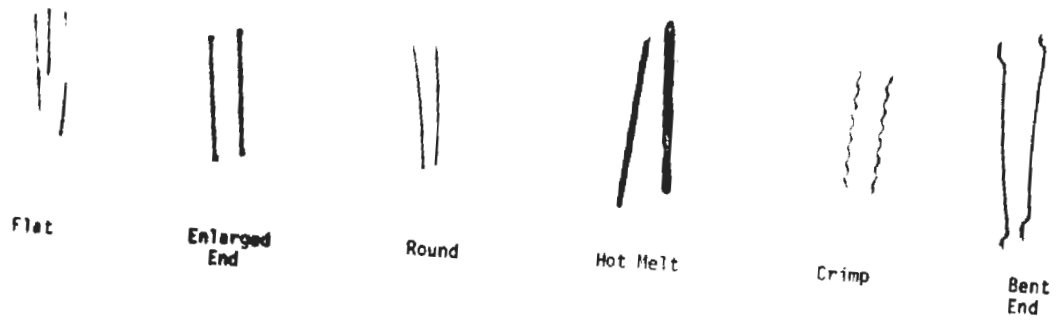

FIG. 2.1 STEEL FIBERS

concrete. The mixes reported in Tables 2.4 and 2.5 were designed for a slump of 4 to 5 in. (100 to 125 mm) for each fiber content. Three plain concrete mix designs were formulated for comparison with the fibrous mixes. From data taken during the casting of fibrous mix designs F, I, H, R, and W, representative slumps of the 0.9 and 1.5 percent series were determined as 6 in. and 5 in. (150 mm and 125 mm) respectively. From this basis two different approaches were taken in obtaining similar workability, as represented by the slump test. The 'S' mix design was based on the same cement content as the fibrous mixes, with water adjusted to yield the desired slump. The 'P' mix design was based on the same water-cement ratio as the fibrous mixes, with a lower cement content. For the 'M' mix design, the fibrous mix designs were used with the omission of fiber.

2.3 FABRICATION AND CURING

2.3.1 TEST SPECIMENS

For the determination of the tensile stress-strain relationship from flexural tests, 4 in. by 6 in. by 64-in. (100 mm by 150 mm by 1625-mm) prisms were cast in molds which consist of rolled steel channel sections hinged and securely bolted together. Prior to each use the forms were cleaned, oiled, and fresh high-strength gypsum plaster placed in the region of the joints between channels to prevent the loss of paste. When the bolts holding the channels together were secured, excess material was forced out of the joint and removed by hand from the mold. The joints were than sealed with the hardening of the plaster.

TABLE 2.4

MIX DESIGNS FOR 0.9 PERCENT SERIES

Mix	Water-cement ratio	Mix material, lb/cu yd (kg/m^3)					
		Water	Cement	Fly ash	Sand	Gravel	Fiber
F,H,I, R,W,B	0.51	336 (200)	660 (392)	222 (132)	1800 (1068)	771 (458)	120 (71)
M	0.51	336 (200)	660 (392)	222 (132)	1800 (1068)	771 (458)	-
P	0.49	316 (187)	644 (382)	217 (129)	1908 (1132)	818 (485)	-
S	0.46	303 (180)	660 (392)	222 (132)	1800 (1068)	771 (458)	-

TABLE 2.5

MIX DESIGNS FOR 1.5 PERCENT SERIES

Mix	Water-cement ratio	Mix material, lb/cu yd (kg/m^3)					
		Water	Cement	Fly ash	Sand	Gravel	Fiber
F,H,I R,W,B	0.49	352 (209)	720 (427)	230 (136)	1860 (1103)	620 (368)	200 (119)
M	0.49	352 (209)	720 (427)	230 (136)	1860 (1103)	620 (368)	-
P	0.49	334 (198)	682 (405)	224 (133)	2012 (1194)	669 (397)	-
S	0.44	319 (189)	720 (427)	230 (136)	1860 (1103)	620 (368)	-

Control specimens for compressive strength and modulus of rupture were 4-in. diameter by 8-in. (100-mm by 200-mm) cylinders and 3 in. by 3 in. by 15-in. (75 mm by 75 mm by 380-mm) prisms, respectively, meeting the requirements of ASTM C 192.

Specimens for direct tension tests were cast in steel prism molds 3 in. by 3 in. by 10 in. (75 mm by 75 mm by 250 mm) with special inserts providing a 2-in. (50-mm) center region with a resulting nominal reduced cross section of 1.5 in. by 3 in. (40 mm by 75 mm). A 5/8-in. (15-mm) diameter threaded rod with a 1/4-in. (5-mm) diameter rod welded perpendicular to the end was held in position during casting by nuts on either side of the mold end plate.

2.3.2 PREPARATION OF SPECIMENS

For each fiber geometry and reinforcement percentage a minimum of two large beams was cast. Mixer capacity precluded casting all large beams from one batch. A batch size of 1.75 cu ft (0.05 m^3) was specified to allow for one large beam, three cylinders and three modulus of rupture beams from each batch. A minimum of three direct tension specimens was cast for each mix design. Batch size allowed casting three tension specimens or performing unit weight and air content tests on the fresh concrete.

A countercurrent rapid batch mixer was used for the mixing of all concrete. Aggregate, cement and fly ash were weighed into the mixing bowl and mixed dry. Fiber was added to the mix through a vibrating screen and chute. Fiber balls, if any, were broken manually and the fiber returned to

the mix. Water was added after a uniform distribution was achieved. Mixing was continued until the mix was homogeneous. The mixer was then stopped and a slump taken. Unit weight and air tests were performed on alternate batches as noted.

Test specimens were immediately cast and vibrated externally. Specimens were struck off and finished with a float, covered with wet burlap and polyethelene after initial set of the paste, and stripped from the molds 22 to 26 hr after casting. After removal from the molds, specimens were placed in a moist room meeting ASTM C 511 until immediately prior to testing.

2.3.3 SPECIMEN IDENTIFICATION

Specimens were identified as to fiber type, as described in Table 2.3, fiber content for which the mix was designed, specimen type (B = modulus of rupture, C = cylinder, F = large flexural specimen, T = tension), and specimen number. For example, RO.9F1 was the first specimen cast with 0.9 volume percent of round fibers. Mixes are referenced by fiber type or fiber type and content.

2.4 TESTING PROCEDURE

2.4.1 CONTROL SPECIMENS

Modulus of rupture beam specimens were tested in accordance with ASTM C 78, except specimens were tested in the position in which they were cast. Cylinders were tested in accordance with ASTM C 39.

2.4.2 DIRECT TENSION SPECIMENS

Direct tension specimens were tested immediately after removal from the moist room. Specimens were fixed in the testing machine by means of universal joint linkages screwed onto the rods embedded in the test specimen. This arrangement reduced eccentricity of the applied load although it cannot be eliminated. The testing machine was operated in stroke control. A stroke rate of 0.005 in./min (0.13 mm/min) was used until after the point of initial cracking. The test was then momentarily stopped while the stroke rate was increased to 0.036 in./min (0.91 mm/min), then continued. This was necessary because the testing machine allows constant stroke rate for 500 sec, then must be reset if further deformation is desired. Tests were terminated at fracture, at a total head travel of 0.3 in. (7.6 mm), or when a plateau was reached at very low load. During the test, load and stroke were automatically recorded with a plotter. Stroke measurement was employed to give a coarse estimation of strain without extensive use of electric strain gages.

2.4.3 LARGE BEAM SPECIMENS

Beam specimens for the determination of the tensile stress-strain relationship were tested as soon as feasible after removal from the moist room. The minor delay was in fastening the measuring system to the specimen.

A sketch of the loading apparatus appears in Fig. 2.2.

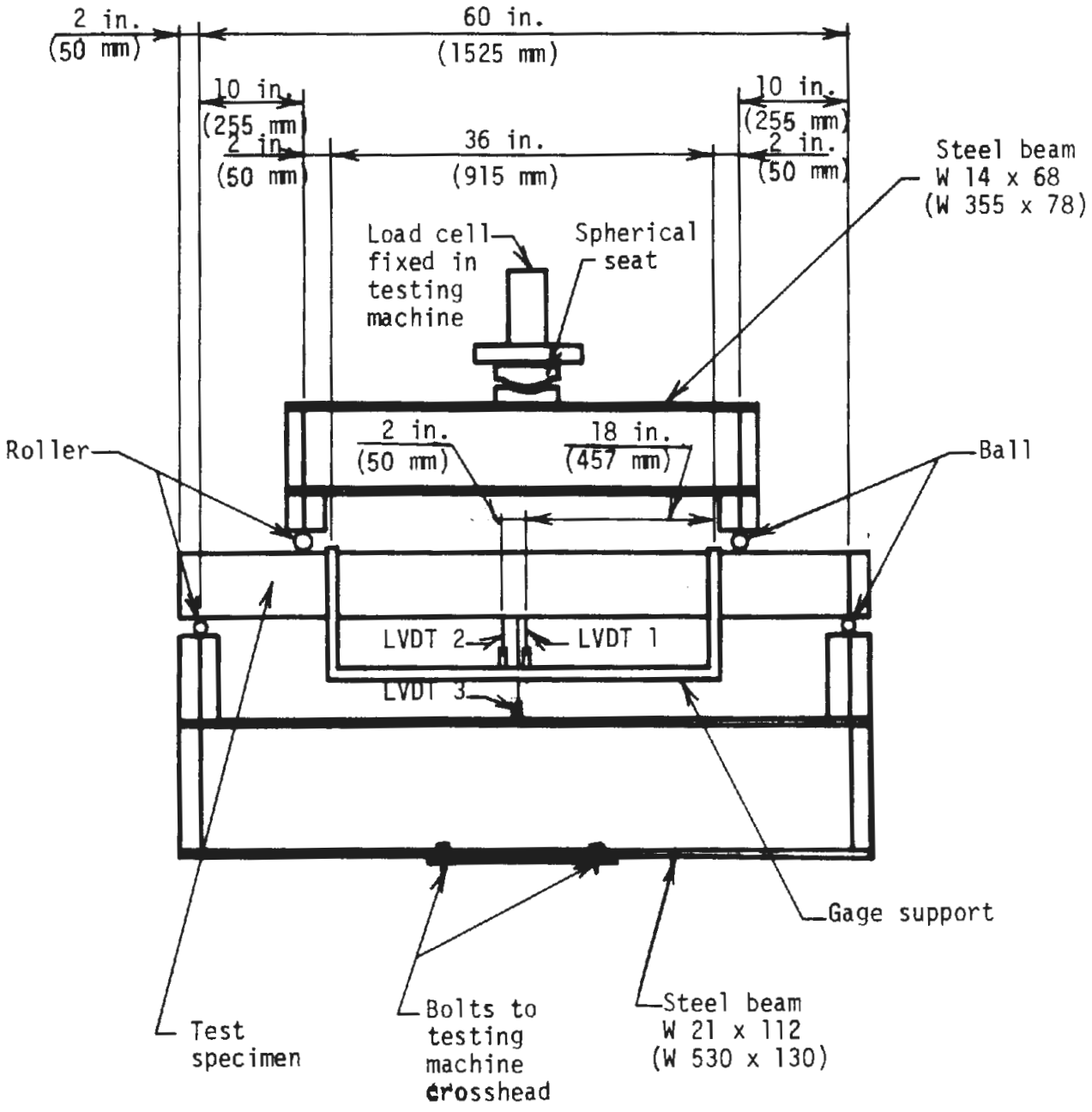

FIG. 2.2 LOADING APPARATUS

The bottom of the loading jig was bolted to the testing machine. The upper part of the jig was placed on top of the specimen and load applied through a spherical seat. A stroke rate of 0.03 in./min (0.8 mm/min) was used for the entire test.

To obtain deflection measurements from the elastic range to failure, three linear variable differential transformers (LVDT's) were employed. LVDT 1, mounted at midspan, measured relative deflection within the constant moment region to a maximum of 0.030 in. (0.75 mm). LVDT 2, offset 2 in. (50 mm) from midspan, measured relative deflection within the constant moment region for the full range of deflection. LVDT 3, mounted at midspan, measured absolute deflection of the specimen with respect to the base of the test jig for the full range of deflection. A 20000 lbf (90 kN) load cell was used for measurement of applied load. The output of a sonic transducer taped to the specimen near the third point was used as input to a digital counter. Disturbance of the specimen through seating or cracking causes an advance of the recorded count.

The three deflection measurements, load, and cumulative count were recorded in analog form during the test and also digitized with a sampling rate of 100/min. Load-deflection for each LVDT and load-count were plotted during the test.

2.5 STANDARD TESTS AND SPECIFICATIONS

The following list serves as a reference for cited standards of the American Society for Testing and Materials [2]:

C 39-72 Standard Method of Test for Compressive Strength of Cylindrical Concrete Specimens;

C 78-64 Standard Method of Test for Flexural Strength of Concrete (Using Simple Beam with Third-Point Loading);

C 138-74 Standard Method of Test for Unit Weight, Yield, and Air Content (Gravimetric) of Concrete;

C 192-69 Standard Method for Making and Curing Concrete Test Specimens in the Laboratory;

C 231-73 Standard Method of Test for Air Content of Freshly Mixed Concrete by the Pressure Method;

C 511-73 Standard Specification for Moist Cabinets and Rooms Used in the Testing of Hydraulic Cements and Concretes; and

C 618-73 Standard Specification for Fly Ash and Raw or Calcined Natural Pozzolans for Use in Portland Cement Concretes.

CHAPTER 3

RESULTS AND ANALYSIS

3.1 FRESH MIX PROPERTIES

Although the study of fresh mix properties was not a major purpose of the investigation, certain observations are of general interest. Fresh mix properties are included in Table 3.1.

Slumps of fibrous mixes varied from 3-1/4 in. to 6-3/4 in. (95 to 170 mm). Air contents were in the range of 3 to 4.5 percent. Air content and slump are insensitive to the type of fiber used.

Observed and theoretical unit weights are compared in Table 3.2. In all cases the observed values are at least 98.5 percent of theoretical. The plain concrete mix designs 'P' and 'S' are denser than the matrix of the fibrous mixes, as represented by mix design 'M', but the percentage increase is slight. If it were possible to compare these densities with the actual matrix density of the fibrous mixes, the difference would likely be greater, due to the effect of the fibers in impeding compaction.

Although balling was not overly severe with any of the fibers, some difficulties were experienced with the crimped and hot melt fibers.

The bent-end fiber is normally supplied in clips of two to ten fibers which are supposed to disperse upon wetting and mixing. Examination of broken specimens later revealed that occasionally groups of a few fibers would remain together.

TABLE 3.1

PROPERTIES OF FRESH AND HARDENED CONCRETE

Mix	Slump, in. (mm)	Unit Weight, lb/cu ft (kg/m^3)	Air, percent	f'_c,[1] psi (MPa)	f'_r,[1] psi (MPa)	f^*_r,[1] psi (MPa)	f'_t,[1] psi (MPa)
F0.9-1	5 (125)	143.4 (2297)	3.6	8060 (55.57)	1155 (7.96)	730^{37} (5.03)	650^{32} (4.48)
-2	6 (150)	--	---	7540 (51.99)	1035 (7.14)	615^{37} (4.25)	---
-3	6-1/4 (160)	144.4 (2313)	3.3	7870 (54.27)	1195 (8.25)	925 (6.39)	350^{2} (2.41)
-4	6-1/4 (160)	--	---	7140 (49.22)	1080 (7.45)	775 (5.35)	--
F1.5-1	4-3/4 (120)	144.9 (2320)	3.3	8090 (55.78)	1230 (8.48)	1010 (6.96)	655^{31} (4.52)
-2	4-1/4 (110)	--	---	8410 (57.98)	1290 (8.89)	1015 (6.99)	--
-3	3-3/4 (95)	145.9 (2336)	3.1	8370 (57.71)	1160 (8.00)	865 (5.96)	--
-4	6 (150)	147.3 (2360)	3.5	7590 (52.31)	1185 (8.15)	910 (6.27)	--
-5	6 (150)	--	-	7660 (52.79)	1340 (9.23)	965 (6.65)	645 (4.43)
I0.9-1	5-1/4 (135)	--	-	7650 (52.74)	1030 (7.10)	820 (5.65)	630^{31} (4.33)
-2	5-1/4 (135)	142.9 (2289)	4.2	7690 (53.02)	1160 (8.00)	810 (5.58)	--
I1.5-1	5-1/2 (140)	--	-	8160 (56.23)	1115 (7.69)	810 (5.59)	655 (4.54)
-2	4-3/4 (120)	142.9 (2289)	4.3	7860 (54.21)	1110 (7.65)	860 (5.92)	--
H0.9-1	6-1/2 (165)	144.4 (23.3)	3.0	7670 (52.88)	915 (6.31)	795 (5.48)	670^{30} (4.61)
-2	6-1/2 (165)	--	-	7830 (53.99)	960 (6.62)	775 (5.34)	--
H1.5-1	5 (125)	145.4 (2329)	3.4	8110 (55.90)	1005 (6.94)	735 (5.06)	--
-2	5 (125)	--	-	8060 (55.58)	1125 (7.77)	730 (5.02)	600 (4.12)
R0.9-1	6-1/4 (160)	--	-	7160 (4941)	1105 (7.61)	835 (5.76)	670^{29} (4.60)
-2	5-3/4 (145)	143.9 (2305)	3.5	7820 (53.93)	1130 (7.78)	710 (4.90)	--
R1.5-1	6 (150)	--	-	8010 (55.26)	1315 (9.06)	830 (5.71)	595 (4.11)
-2	5-1/2 (140)	146.8 (2352)	3.0	8270 (57.00)	1350 (9.32)	1040 (7.18)	--

[1] Test age other than 28d noted in superscript.

TABLE 3.1 (Continued)

Mix	Slump, in.(mm)	Unit Weight, lb/cu$_3$ft (kg/m^3)	Air, percent	f'_c,[1] psi(MPa)	f'_r,[1] psi(MPa)	f^*_r,[1] psi(MPa)	f'_t,[1] psi(MPa)
W0.9-1	5-1/2 (140)	145.9 (2336)	3.0	8130 (56.04)	1080 (7.45)	685 (4.75)	590 (4.07)
-2	6-3/4 (170)	--	-	8190 (56.45)	895 (6.69)	615 (4.24)	--
W1.5-1	6 (150)	145.4 (2329)	3.0	7980 (54.99)	1100 (7.57)	815 (5.61)	--
-2	6 (150)	--	-	8040 (55.44)	1185 (8.19)	720 (4.95)	720 (4.95)
B0.9-1	6 (150)	143.4 (2297)	4.0	7080 (48.84)	1185 (8.18)	935 (6.46)	--
-2	5-1/2 (140)	--	-	7550 (52.06)	1705(11.75)	820 (5.66)	545 (3.75)
B1.5-1	3-1/4 (85)	--	-	7310 (50.37)	1585(10.92)	1000 (6.89)	710 (4.90)
-2	4-1/2 (115)	144.4 (2313)	4.4	7070 (48.72)	1685(11.63)	915 (6.30)	--
S0.9-1	5-1/2 (140)	--	-	7860 (54.16)	995 (6.87)	710 (4.88)	630 (4.34)
-2	4 (100)	142.0 (2274)	4.2	7840 (54.03)	945 (6.50)	750 (5.17)	--
-3	4-1/2 (115)	142.9 (2289)	4.0	8430 (58.10)	1040 (7.17)	755 (5.22)	--
S1.5-1	5 (125)	142.0 (2274)	4.1	8600 (59.29)	1145 (7.89)	850 (5.86)	--
-2	4-1/4 (110)	--	-	8860 (61.12)	1025 (7.08)	805 (5.56)	660 (4.54)
-3	4-1/2 (115)	--	-	8090 (55.76)	1135 (7.81)	720 (4.96)	630 (4.35)
M0.9-1	8 (200)	--	-	7800 (53.75)	1035 (7.13)	735 (5.06)	615 (4.24)
-2	8 (200)	141.5 (2266)	4.0	7250 (50.00)	1035 (7.13)	780 (5.40)	--
M1.5-1	8-1/4 (210)	141.5 (2266)	2.7	7860 (54.21)	1025 (7.08)	835 (5.75)	--
-2	7 (180)	--	-	8030 (55.40)	995 (6.87)	840 (5.81)	615 (4.23)
P0.9-1	5-3/4 (145)	141.5 (2268)	4.1	7870 (54.25)	1040 (7.17)	740 (5.09)	--
-2	6 (150)	--	-	7440 (51.28)	965 (6.65)	700 (4.84)	580 (4.01)
P1.5-1	5-1/4 (135)	141.0 (2258)	4.1	7780 (53.61)	1005 (6.94)	820 (5.65)	--
-2	5-1/4 (135)	--	-	7300 (50.37)	980 (6.77)	775 (5.33)	560 (3.97)

[1]Test age other than 28d noted in superscript.

TABLE 3.2

OBSERVED AND THEORETICAL UNIT WEIGHT

	Unit weight wet, lb/cu ft (kg/m^3)			
	0.9 Percent series		1.5 Percent series	
Mix	Observed	Theoretical	Observed	Theoretical
Fibrous	144.0 (2307)	145.3 (2327)	145.4 (2329)	146.8 (2352)
M	141.5 (2267)	142.2 (2278)	141.5 (2267)	141.6 (2268)
S	142.5 (2283)	143.9 (2305)	142.0 (2275)	143.3 (2995)
P	141.5 (2267)	143.7 (2302)	141.0 (2259)	142.9 (2289)

3.2 STRENGTH

Various strength parameters provide useful insight into material behavior and standards for comparison, although proper interpretation is required. Mean strengths of compression cylinders (f'_c), modulus of rupture beams (f'_r), large beams (f^*_r), and direct tension specimens (f'_t) are tabulated in Table 3.1 for each batch.

Comparison of the cylinder test results for the different fibers and fiber contents, Figs. 3.1 and 3.2, indicates the general nature of these concretes in a manner most familiar to engineers. Typically the concretes are of high strength, in the range of 7000-8000 psi (50-55 MPa). For most fiber geometries the strength of the mix containing 1.5 percent fiber is on the

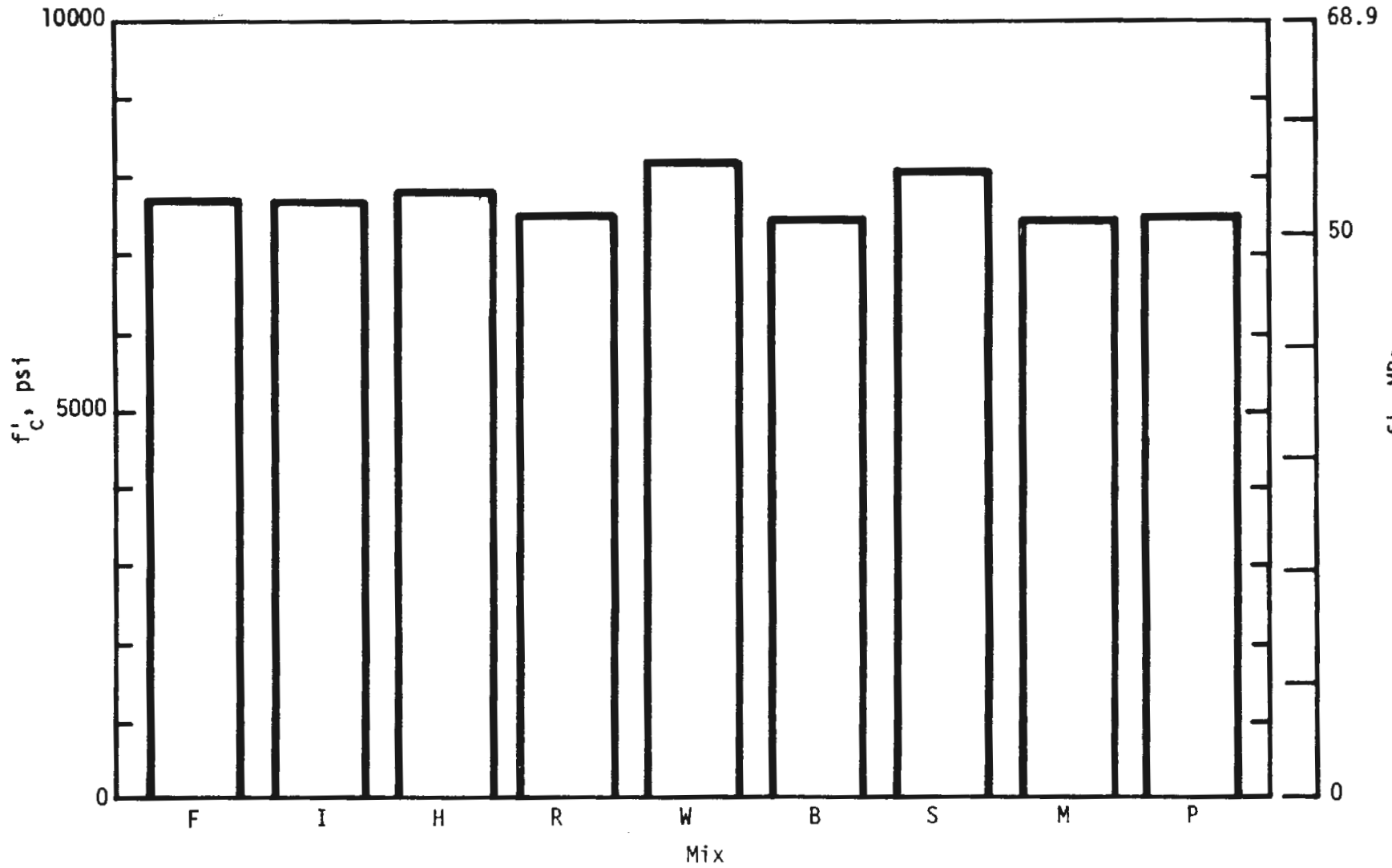

FIG. 3.1 COMPRESSIVE STRENGTH FOR CONTROL SPECIMENS, 0.9 PERCENT SERIES

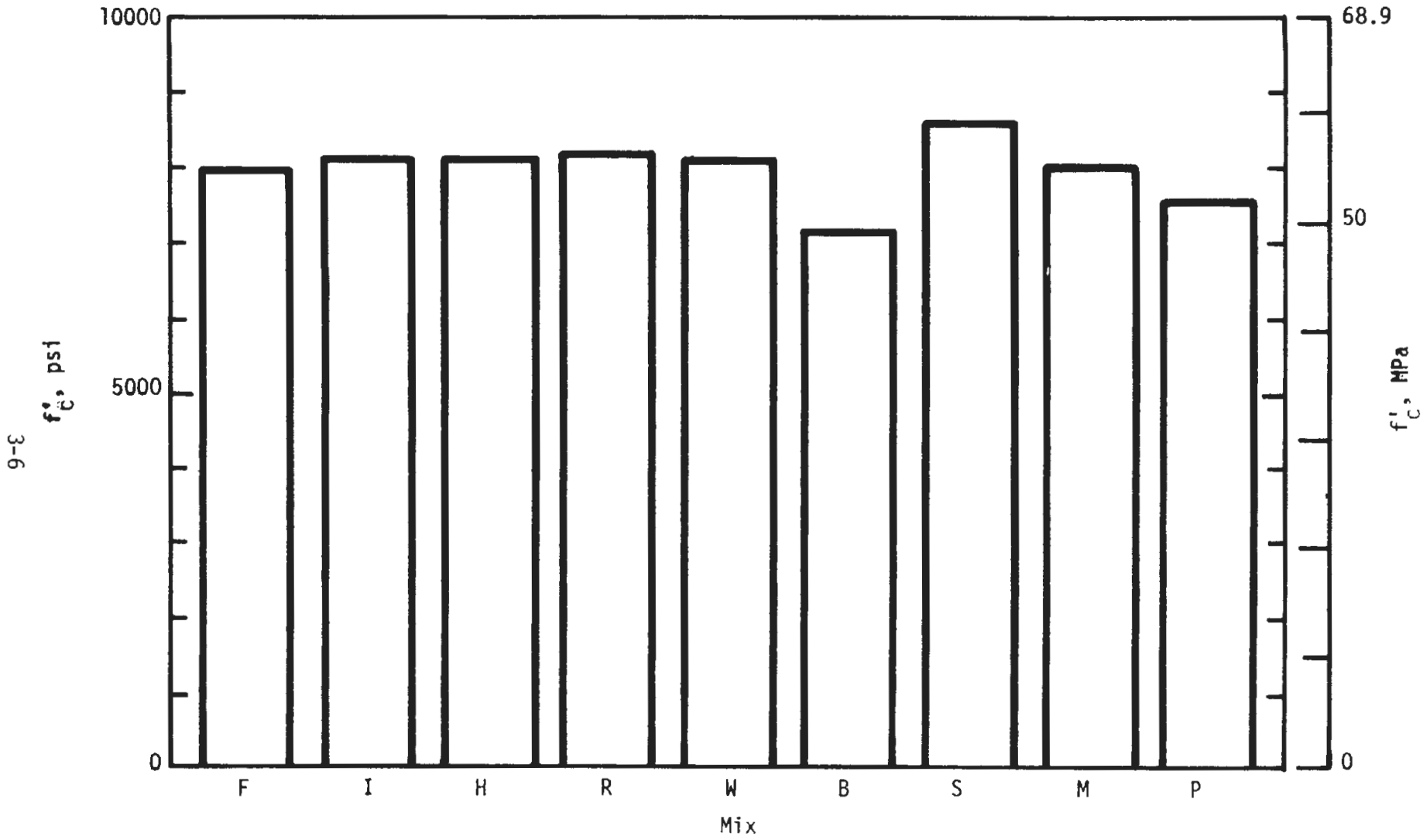

FIG. 3.2 COMPRESSIVE STRENGTH FOR CONTROL SPECIMENS, 1.5 PERCENT SERIES

order of 500 psi (3.5 MPa) higher than the 0.9 percent mix. Generally, the fiber reinforced concretes were only slightly higher in strength than the appropriate 'M' plain concrete mix.

For the plain concretes, the 'S' series had higher strengths than the 'M' series at both fiber contents, a consequence of reduced water-cement ratio at the same cement content. For the 0.9 percent mixes, the 'P' series were slightly higher in strength than the 'M' series but for the 1.5 percent mixes, the 'M' series was higher. It was expected that the 'M' series be of higher strength because of its greater cement content at the same water-cement ratio.

Strength in flexure was determined by computing a nominal modulus of rupture from tests of 3 in. by 3 in. by 15-in. (75 mm by 75 mm by 380-mm) and 4 in. by 6 in. by 64-in. (100 mm by 150 mm by 1625-mm) beams. Examination of Figs. 3.3 through 3.6 shows certain trends in behavior, but an absolute ranking of behavior on the basis of modulus of rupture is not possible. For the control specimens, strengths of the 1.5 percent mixes were typically less than 200 psi (1.4 MPa) greater than the 0.9 percent mixes for the same fiber geometry. Except for the bent-end fiber, strengths with the deformed fibers were actually lower than with the round or flat straight fibers. Mixes in the 0.9 percent series with hot melt and crimped fibers were lower in strength than the 'M' plain mix. Other fibers yielded strengths 10 to 40 percent greater than for the 'M' mix. Fibrous mixes in the 1.5 percent series exceeded the strength of the 'M' mix by 5 to 60 percent.

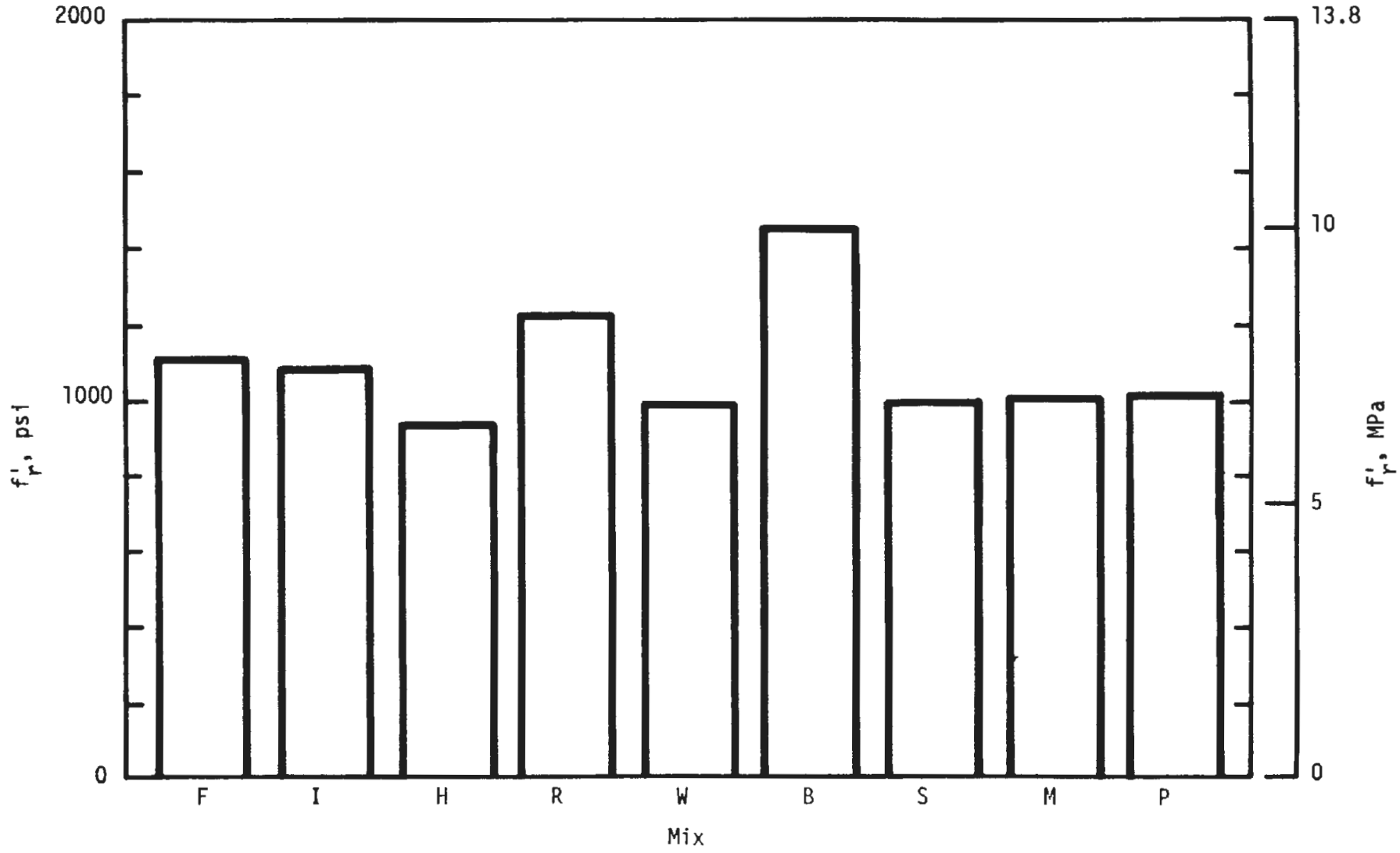

FIG. 3.3 MODULUS OF RUPTURE FOR CONTROL SPECIMENS, 0.9 PERCENT SERIES

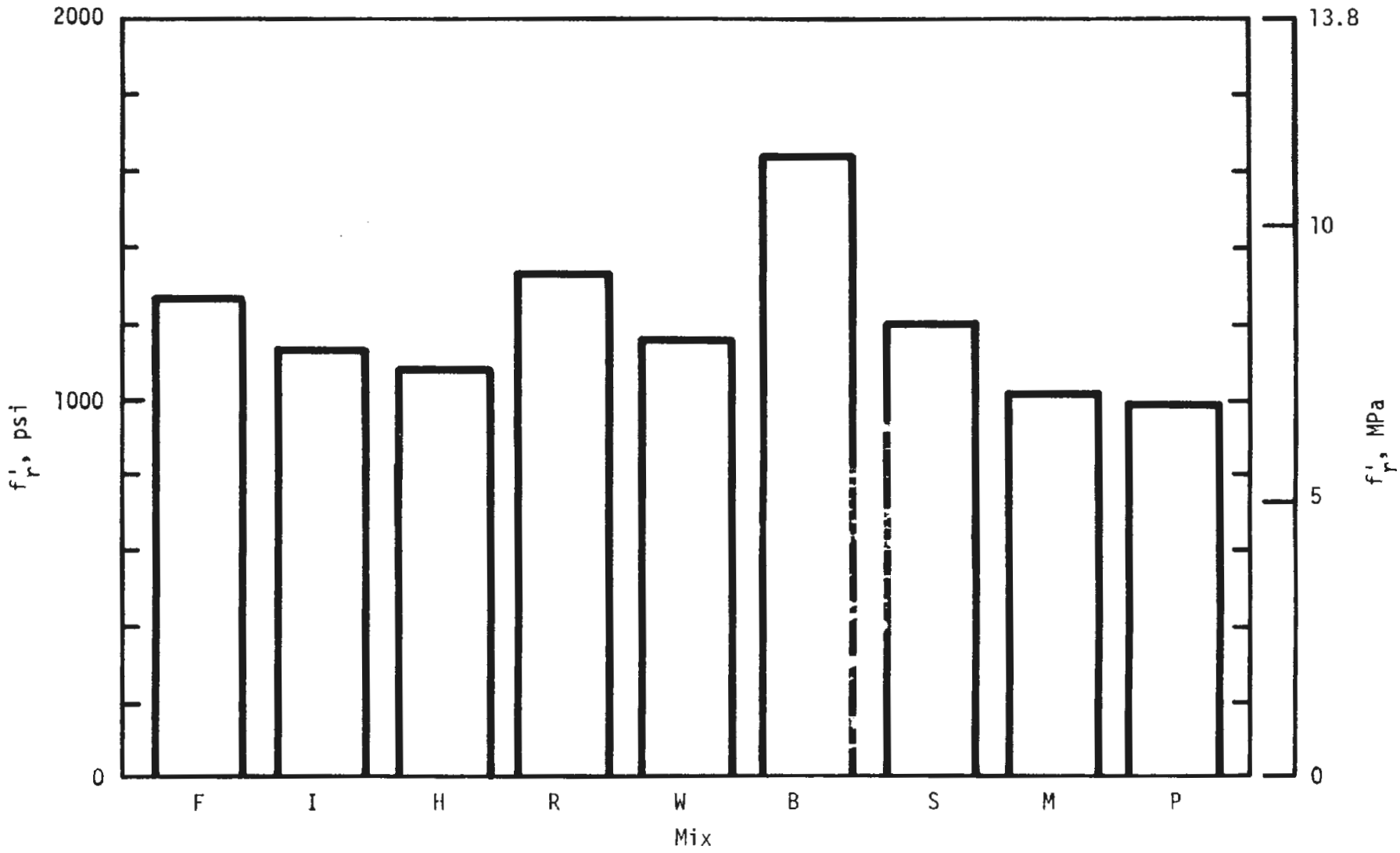

FIG. 3.4 MODULUS OF RUPTURE FOR CONTROL SPECIMENS, 1.5 PERCENT SERIES

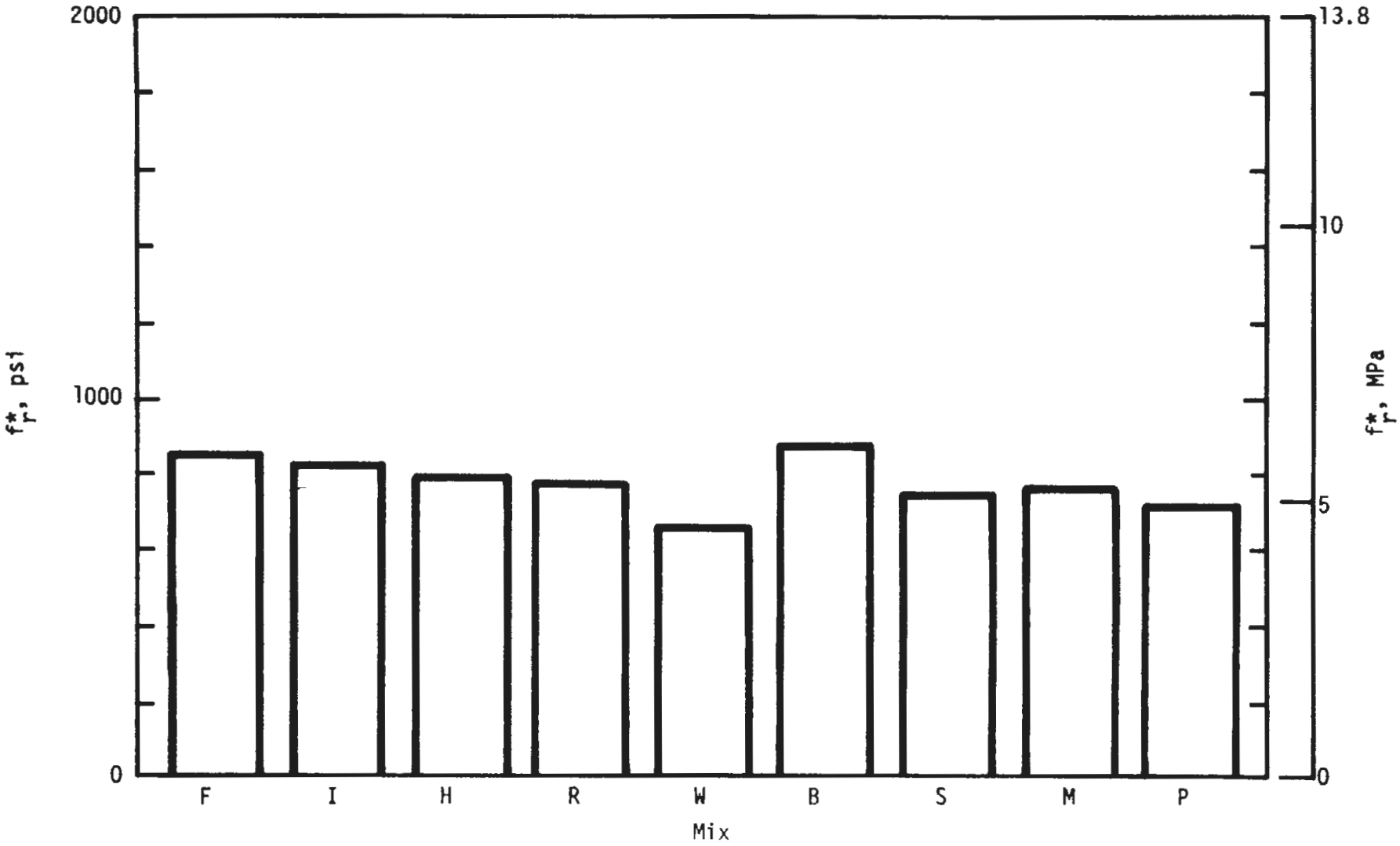

FIG. 3.5 MODULUS OF RUPTURE FOR LARGE BEAMS, 0.9 PERCENT SERIES

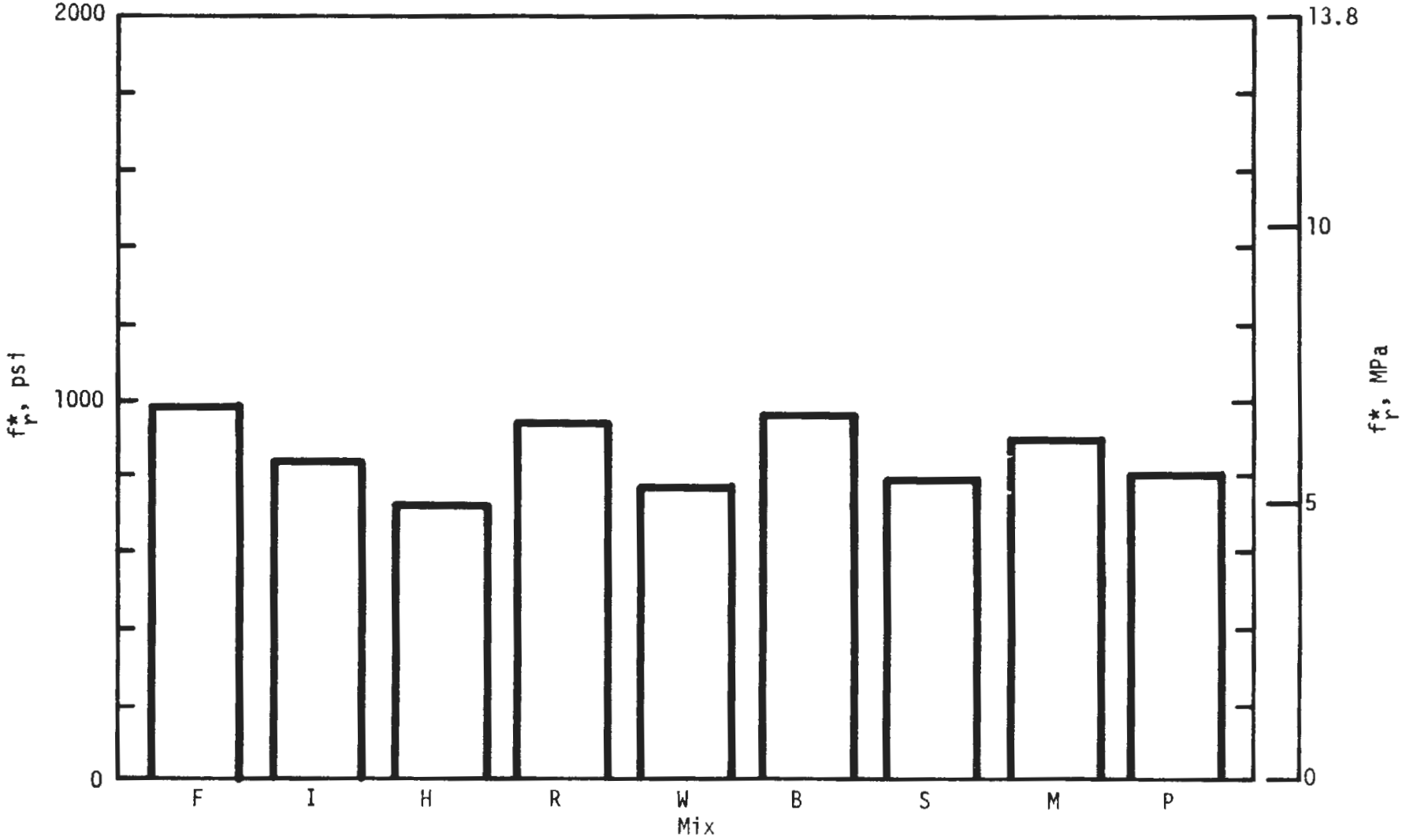

FIG. 3.6 MODULUS OF RUPTURE FOR LARGE BEAMS, 1.5 PERCENT SERIES

The flexural strengths computed from tests of the large beams are significantly lower than from tests of the control specimens. Considering all tests of control specimens and large beams in this investigation, the mean strength decline was 31 percent for fibrous mixes and 25 percent for plain mixes. Herring, et al., [8] reported a mean strength difference of 28 percent for 6 in. by 6 in. by 64-in. (150 mm by 150 mm by 1625-mm) beams cast with a different cement and mix design.

For the larger specimens, fibrous mixes show only limited strength increase over the 'M' plain mix, and the number of instances for which the fibrous mix is actually lower is increased. Apparently, the nature of the material flaw distribution is such that the strength of a fibrous mix will approach the strength of the matrix, for some combination of material volume and stress state. Strengths of fiber reinforced mixes less than the matrix strength can probably be attributed to regions of poor compaction due to the presence of fiber. A further consideration is the increased ratio of least specimen dimension to fiber length with the larger specimens.

Examination of the nominal tensile strength results, Figs. 3.7 and 3.8, provides information into specimen behavior which can be applied to other situations with great caution. Tension tests of concrete must be recognized as having highly disputable results unless experimental fixtures and techniques are stringently designed and observed. Strengths of all mixes are in the neighborhood of 600 psi (4.1 MPa). No significant strength differences can be assigned to fiber geometry or fiber content.

As important as the actual value of strength is strength reliability. Reliability is best described with a frequency distribution, but a substantial

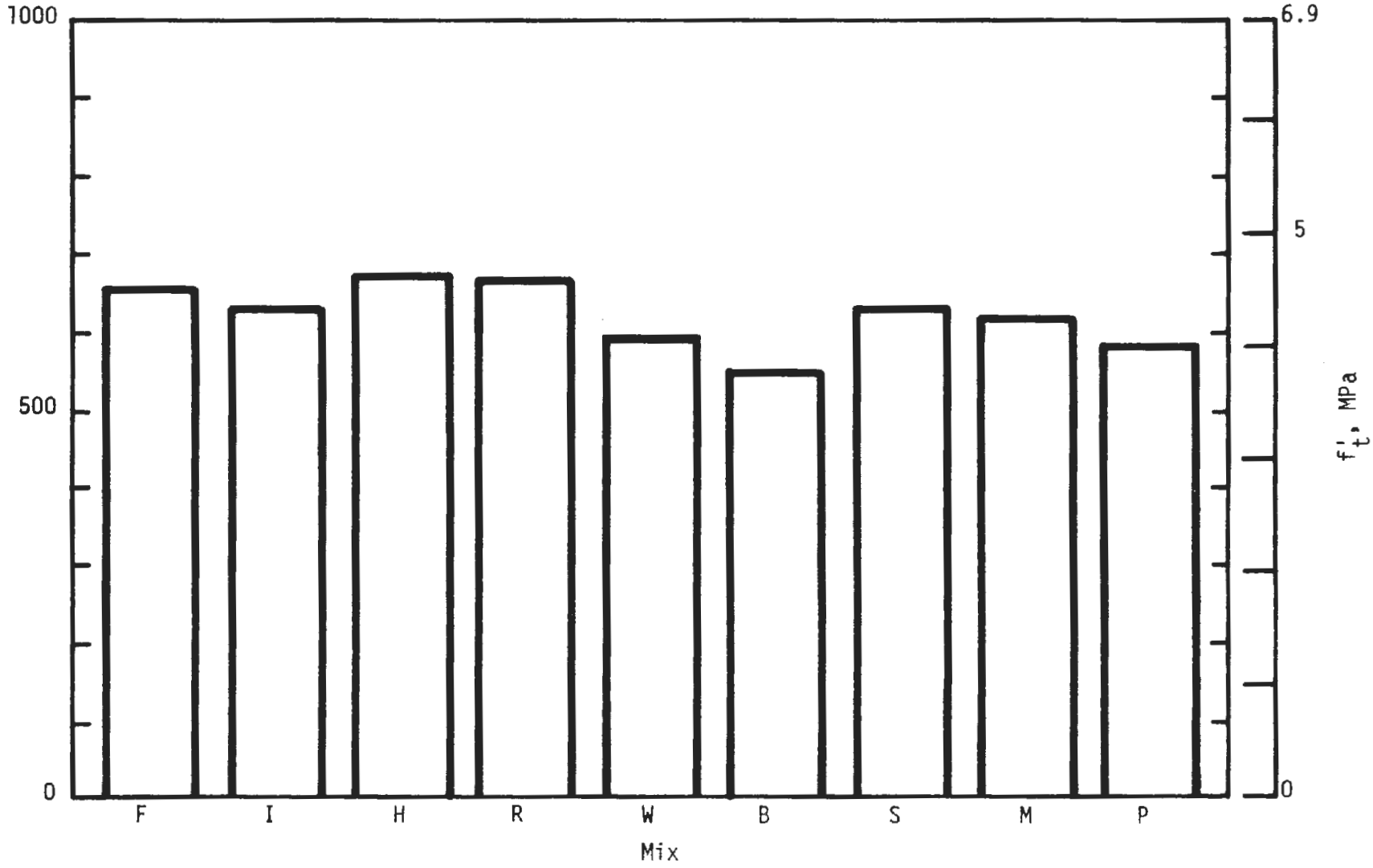

FIG. 3.7 NOMINAL TENSILE STRENGTH, 0.9 PERCENT SERIES

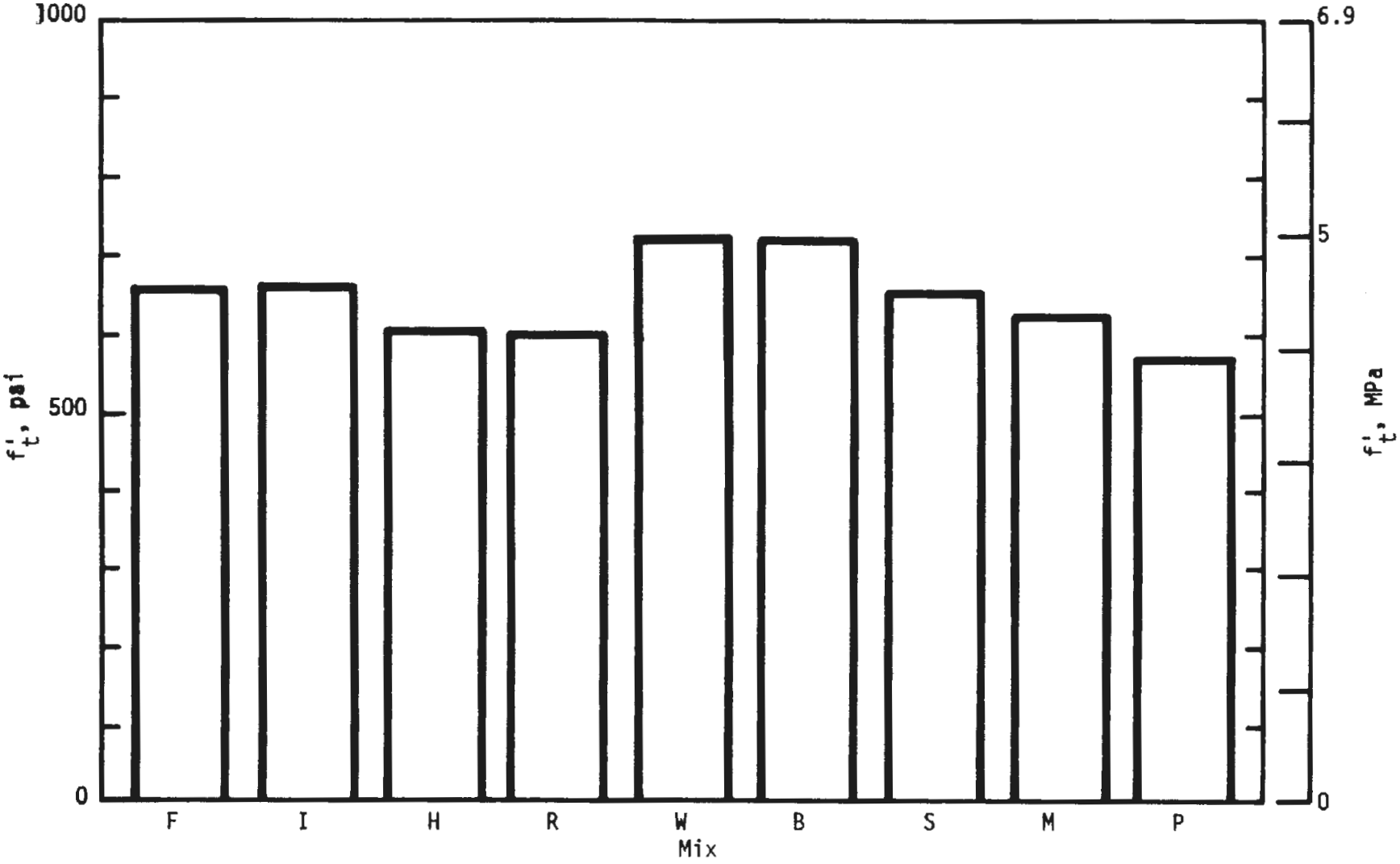

FIG. 3.8 NOMINAL TENSILE STRENGTH, 1.5 PERCENT SERIES

number of tests is required to determine such a distribution. For each mix design considered in this investigation a standard deviation and coefficient of variation were computed for control specimens, Table 3.3. Although significance is limited by sample size, useful observations are possible.

The general trend observable from this data is that strength variability increases with the participation of fibrous reinforcement in overall determination of strength. Variability is thus dependent on loading condition and mode of failure, fiber content, and fiber type. Further, there is increased variability in the flexural control strengths for large beam specimens which exhibit a high degree of ductility.

3.3 LOAD-DEFLECTION RELATIONSHIPS

3.3.1 INTRODUCTION

Consideration of load-deflection relationships can provide a more thorough appreciation of material behavior than is possible by consideration of strength, alone. This is important in the assessment of ductile materials and particularly important in the case of materials for which the ductility can be adjusted. With the addition of fibers, concrete is such a material. Load-deflection behavior may be used to compare the effect of such parameters as fiber content and geometry, the major parameters of this study.

There is, however, an inherent disadvantage to this basis for comparison. Load-deflection behavior pertains to a specific structural element and loading condition. For a test specimen this means that true material behavior is reflected in terms of method and rate of loading, specimen geometry,

TABLE 3.3

STRENGTH RELIABILITY OF MIX DESIGNS

Mix	Compression					Flexure				
	Mean*		Standard deviation,		Coefficient of variation	Mean*		Standard deviation,		Coefficient of variation
	psi	(MPa)	psi	(MPa)		psi	(MPa)	psi	(MPa)	
F0.9	7650	(52.7)[12]	440	(3.0)	0.06	1120	(7.7)[12]	125	(0.9)	0.11
I0.9	7670	(52.9)	275	(1.9)	0.04	1095	(7.5)	90	(0.6)	0.08
H0.9	7750	(53.4)	685	(4.7)	0.09	940	(6.5)	35	(0.3)	0.04
R0.9	7490	(51.7)	600	(4.1)	0.08	1120	(7.7)[5]	70	(0.5)	0.06
W0.9	8160	(56.2)	120	(0.8)	0.01	990	(6.8)	125	(0.9)	0.13
B0.9	7320	(50.5)	320	(2.2)	0.04	1445	(10.0)	440	(3.0)	0.30
S0.9	8040	(55.4)[9]	350	(2.4)	0.04	990	(6.8)[9]	50	(0.3)	0.05
M0.9	7520	(51.9)	445	(3.1)	0.06	1035	(7.1)	70	(0.5)	0.07
P0.9	7650	(52.8)	260	(1.8)	0.03	1000	(6.9)	65	(0.4)	0.07
F1.5	7940	(54.7)[12]	415	(2.9)	0.05	1260	(8.7)[12]	180	(1.2)	0.14
I1.5	8010	(55.2)	360	(2.5)	0.04	1110	(7.7)	165	(1.1)	0.15
H1.5	8080	(55.7)	380	(2.6)	0.05	1065	(7.4)	90	(0.6)	0.08
R1.5	8140	(56.1)	410	(2.8)	0.05	1335	(9.2)	270	(1.9)	0.20
W1.5	8010	(55.2)	295	(2.0)	0.04	1145	(7.9)	100	(0.7)	0.09
B1.5	7220	(49.8)[5]	290	(2.0)	0.04	1630	(11.2)	250	(1.7)	0.15
S1.5	8520	(58.7)[9]	495	(3.4)	0.06	1100	(7.6)	90	(0.6)	0.08
M1.5	7950	(54.8)	315	(2.2)	0.04	1010	(7.0)	105	(0.7)	0.10
P1.5	7540	(52.0)	350	(2.4)	0.05	995	(6.6)	55	(0.4)	0.06

* Mean of 6 specimens unless otherwise indicated in superscript.

and the nature of the test fixtures. The proper interpretation of the results is contingent upon consideration of these factors, either in the design of the experiment, or during the resulting analysis.

With due consideration given to the factors which may influence measured test data, experimentally determined load-deflection relationships can be used to determine section properties, such as moment-curvature relationships for flexure, and material stress-strain properties.

Continual care must be observed in the analytical steps which lead from member to section, and section to material properties. These steps inherently are contingent on a form of numerical differentiation, a process which increases roundoff error. This is familiar from the study of approximate solutions based on assumed deflection shapes where convergence of each higher order derivative is slower.

3.3.2 FLEXURE TESTS

For the instrumented beam tests the test fixtures were chosen to be rigid compared to the test specimen. This minimized deformation of the test specimen at cracking due to release of energy stored in the test fixtures. The stroke rate of 0.03 in./min (0.8 mm/min) used for similar tests by Herring, et al., [8] was adopted for this test series. Further tests by Paul and Ferrera-Boza [17] have suggested that the descending branch of the curve may be better obtained if the loading rate is reduced by half.

The major difficulty in comparing load-deflection curves in this series arises because of the large constant moment region utilized for the instrumentation. The crack seeks the weakest section within the constant

moment region, rupture occurs, and further curvature becomes concentrated at the failure plane in the fashion of a plastic hinge. As the load-deflection relationship is quite sensitive to the crack location, no comparison of behavior will be made directly on the basis of the measured load-deflection curves.

A few general comments on the nature of the load-deflection relationship may be of interest at this point. Typical load-deflection curves as indicated by the three LVDT's are shown in Figs. 3.9-3.11 for specimen RO.9F1. The crack was located 14.75 in. (375 mm) right of midspan, as viewed in Fig. 2.2. The initial portion of the curve is generally very straight in the case of LVDT's 1 and 2, although several specimens showed sharp curves from the outset. The mean modulus of elasticity calculated from the deflection measured by LVDT 1 for each mix design is reported in Table 3.4. Information from LVDT 3 was strongly influenced by seating of the specimen and was curved until relatively high loads were attained. For fibrous specimens a noticeable change in slope of the curve occurred somewhere between 0.5 and 0.8 times the maximum load. This point, termed the proportional limit, is assumed to correspond to initiation of cracking at the macro level. After this point is passed, load continued to increase until a maximum is reached, often the absolute maximum. A variety of responses occurred at this point. All specimens with hot melt fibers fractured, exactly as a plain concrete beam would fail, showing no increase in ductility. Flat and enlarged-end fibers began the descending branch immediately. Round and crimped fibers generally showed an immediate drop of 15 to 25 percent of the maximum load followed by a descending branch with a more gradual slope than the flat or enlarged-end fibers. Several specimens exhibited a load plateau with width on the order of 3 to 4 times the cracking

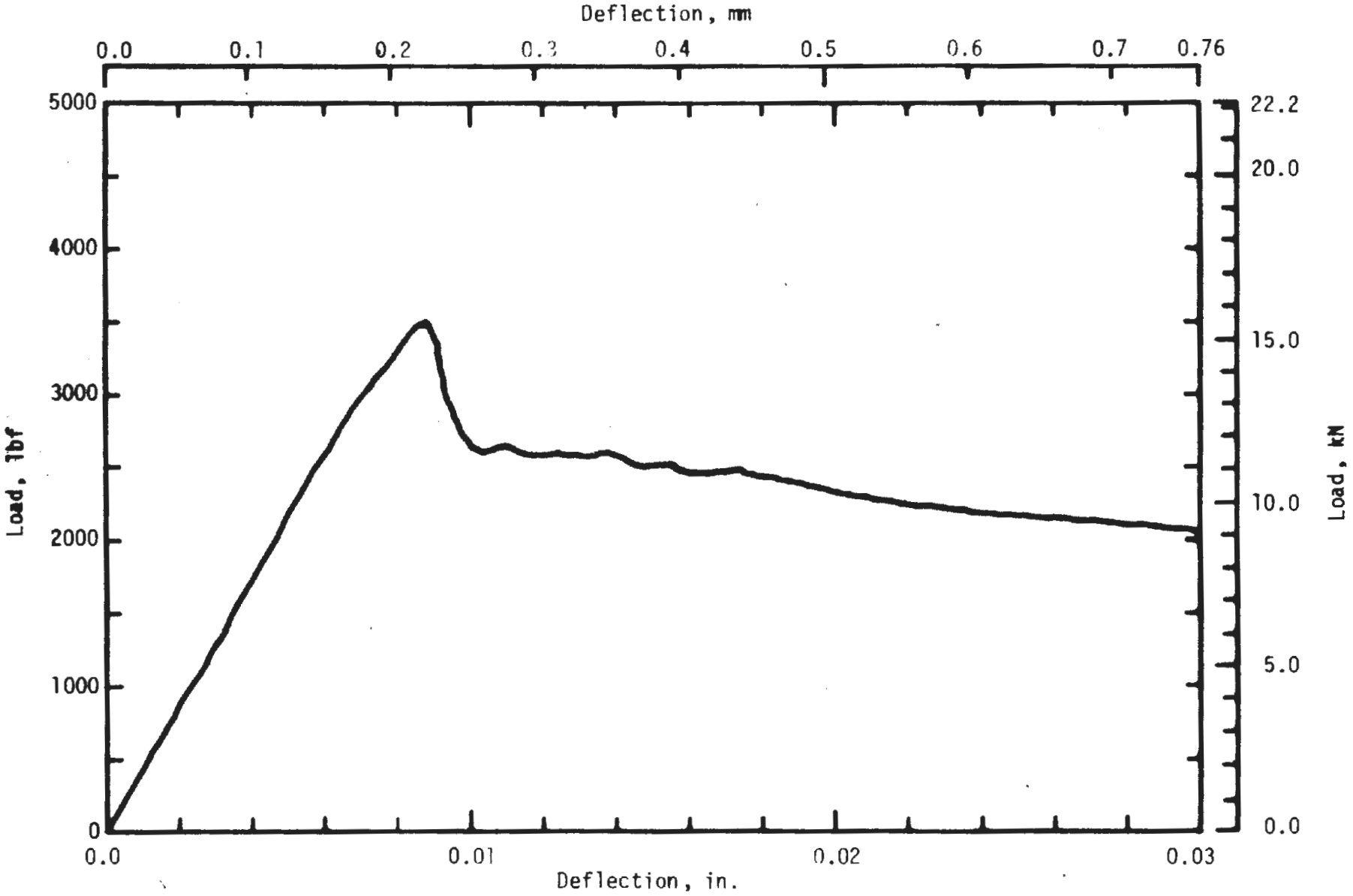

FIG. 3.9 LOAD-DEFLECTION RELATIONSHIP FOR SPECIMEN RO.9 F1, LVDT 1

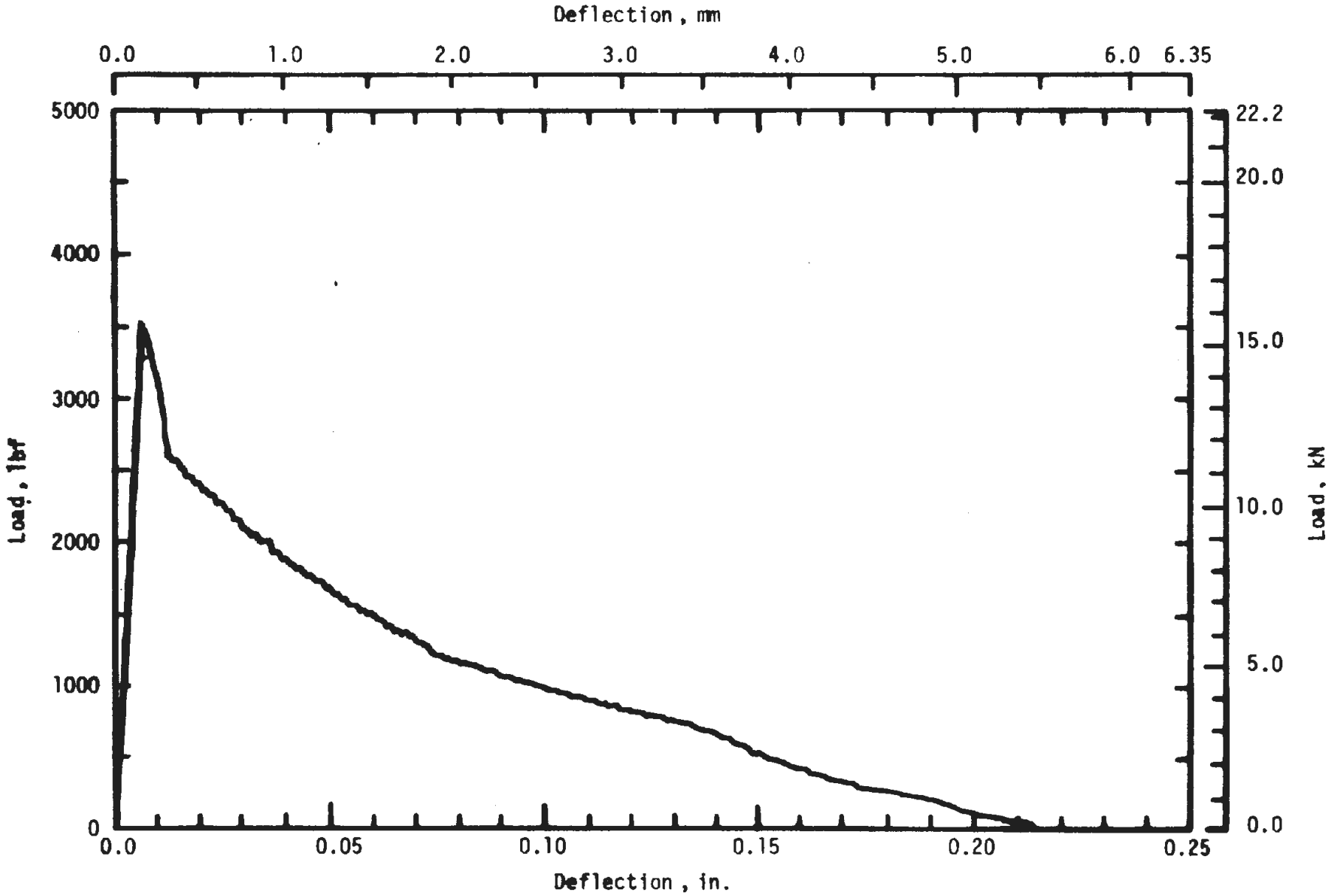

FIG. 3.10 LOAD-DEFLECTION RELATIONSHIP FOR SPECIMEN RO.9 F1, LVDT 2

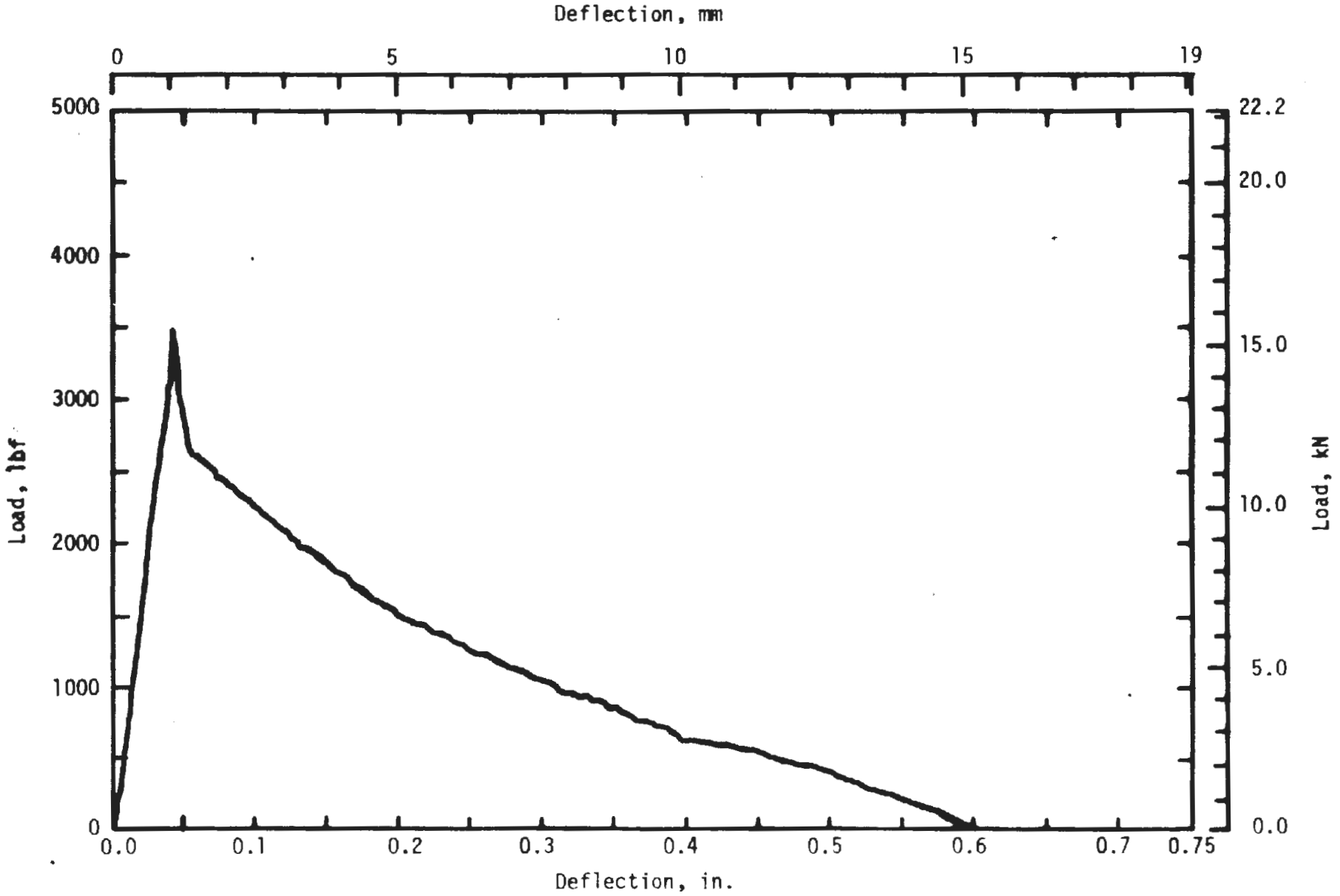

FIG. 3.11 LOAD-DEFLECTION RELATIONSHIP FOR SPECIMEN RO.9 F1, LVDT 3

TABLE 3.4

MODULUS OF ELASTICITY IN FLEXURE

Mix	Modulus of elasticity, psi (GPa)	
	0.9 Percent	1.5 Percent
F	4,390,000 (30.3)	5,210,000 (35.9)
I	4,600,000 (31.7)	4,980,000 (34.3)
H	5,060,000 (34.9)	4,780,000 (33.0)
R	4,340,000 (29.9)	5,110,000 (35.2)
W	4,870,000 (33.6)	4,570,000 (31.5)
B	4,420,000 (30.5)	4,950,000 (34.1)
S	5,000,000 (34.5)	5,090,000 (35.1)
M	5,200,000 (35.9)	5,050,000 (34.8)
P	4,610,000 (31.8)	5,270,000 (36.3)

deflection. For the bent-end fibers a similar initial drop was observed, but followed by a further increase in load which in all cases exceeded the load prior to the sudden drop. Load plateaus of 5 to 7 times the cracking deflection were observed before the onset of the descending branch.

In the case of specimens showing the abrupt drop prior to onset of the descending branch or increase in load, the magnitude of the drop may be of interest. The average drop was 630 lbf (2.8 kN), with the nominal range 125 to 1250 lbf (0.6 to 6.0 kN). Most magnitudes were close to 500 lbf (2.2 kN), which is the weight of the loading jig.

The use of the sonic transducer was intended to aid in determination of the cracking load. Results were erratic and no definite procedures have been developed for applying this technique. In plotting load against cumulative acoustic emission, advances in the emission count can be correlated with a perturbation of the observed load-deflection curve, but no obvious distinctions can be made regarding the cause of the disturbance. The output of the sonic transducer was played through a loudspeaker throughout the test. In the case of specimens with a gently descending branch numerous peaks and valleys are evident in the load-deflection curve. Each drop was coincident with a burst of noise. This is interpreted as a manifestation of individual fibers pulling out of the matrix. The magnitude of these little drops in load is roughly proportional to the pullout strength of individual fibers.

3.3.3 TENSION TESTS

The purpose of the direct tension tests in this study was to provide a check on the stress-strain curves computed from flexural tests. Representative load-deflection curves for each fiber type with 0.9 percent reinforcement are shown in Fig. 3.12. The experimental techniques were not well-refined and were the source of two items of difficulty.

During testing, energy release from the test fixtures at the point of cracking often resulted in severe disruption of the test specimen. In these cases, load dropped to zero, increased somewhat and slowly dropped again as fibers pulled out. This behavior is typified by curve FO.9 in Fig. 3.12. Referring to the same figure, three other curves are shown which describe the extremes in observed behavior. Curve RO.9 is typical of the

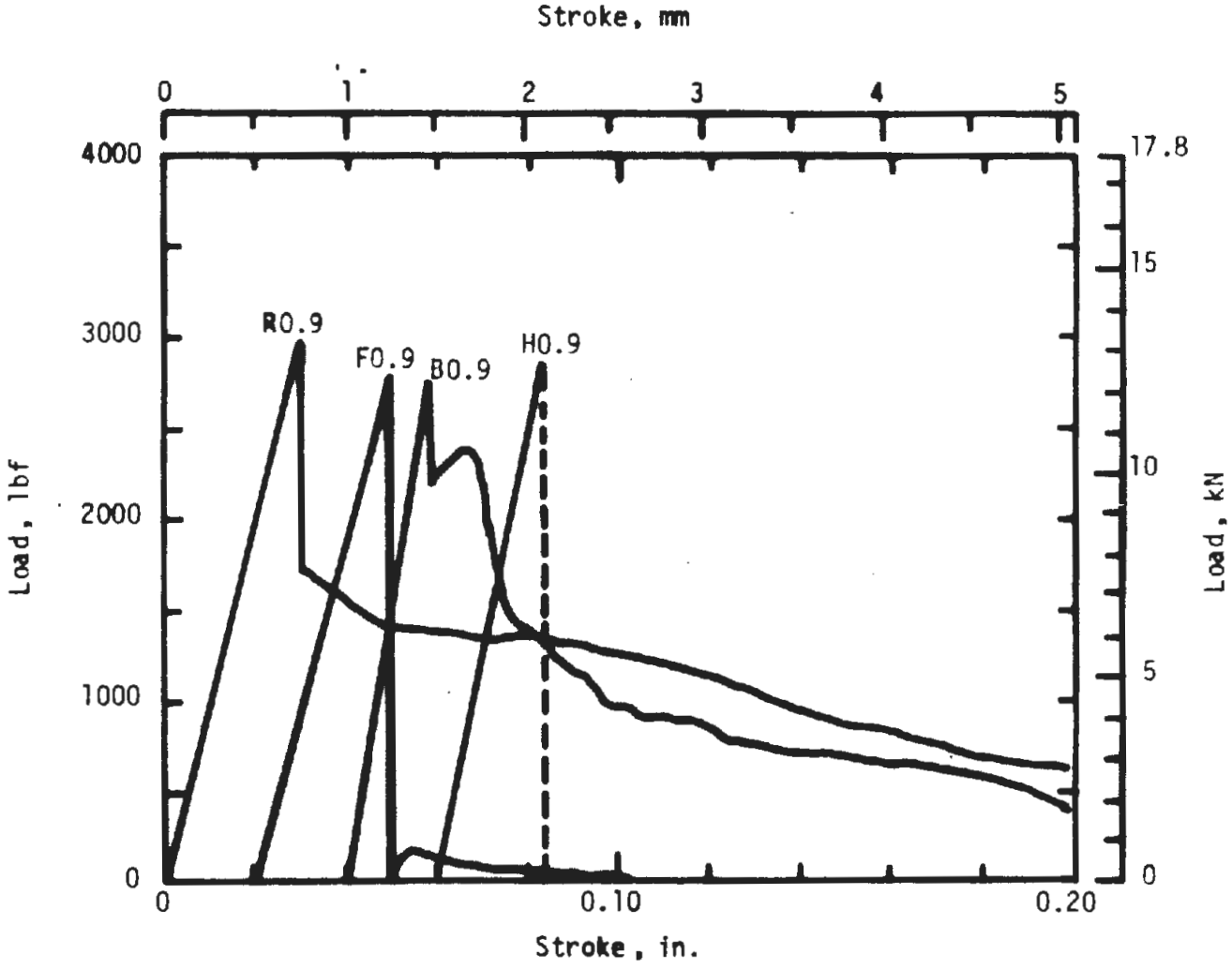

FIG. 3.12 TYPICAL LOAD-DEFLECTION RELATIONSHIPS IN TENSION

shape of most fiber reinforced specimens, although there was much variation in the nature of the descending branch. Curve B0.9 shows evidence of crack arrest followed by increasing load until the onset of fiber pullout. Similar behavior was also observed for some specimens with flat, enlarged-end, and crimped fibers, although in these cases the load drop prior to crack arrest was significantly larger. Curve H0.9 is typical of the hot melt fiber and plain concrete specimens. At the onset of cracking there is virtually no resistance to crack propagation, and the specimens fracture immediately.

A second problem related to test fixture stiffness is evident when attempting to compute an elastic modulus from load-deflection curves. Computations based on the assumption that all deformation occurs within the test specimen lead to a modulus with magnitude substantially less than was observed in the flexure tests. This is a consequence of measuring cumulative stroke of the testing machine head, and thus implies considerable deformation of the test fixture.

In light of the preceding discussion, it is obvious that the tension test series is of primary value in qualitative comparisons. Significant quantitative results would require much more experimental effort than was appropriate for this investigation.

3.4 MOMENT-CURVATURE RELATIONSHIPS

3.4.1 INTRODUCTION

The moment-curvature ($M - \phi$) relationship is a section property, a function of material properties and section geometry, which may be used as a

constitutive relationship in analysis. For traditional analysis of reinforced concrete, the moment-curvature relationship is computed for a section from equilibrium; compatibility of strains between steel and concrete, and known material stress-strain relationships. The computed M - ϕ relationship may be experimentally verified by measuring strains over the depth of the cross section during loading. For fiber reinforced concrete these computations of the M - ϕ relationship are not possible because of the dispersed reinforcement. The experimental procedures would be possible but the volume of material required for casting suitable specimens would be prohibitive for developmental purposes. The moment-curvature relationships can be calculated from experimentally determined load-deflection curves if the material is assumed homogeneous and certain further simplifying assumptions are made.

The computed M - ϕ relationship, and the stress-strain relationship which eventually followed, are calculated only for the material in the immediate vicinity of the failure section. This restriction follows from the obvious argument of strength of the weakest section, and the assumption regarding distribution of curvature along the beam.

By considering deflections only within the constant moment region the problem is simplified. A reasonable assumption for the distribution of curvature is that a uniform distribution of curvature, ϕ_2, exists in the region surrounding a crack, and that ϕ_1 = M/EI along the remainder of the beam, where M is the applied moment, and EI is the elastic flexural rigidity of the section. A length of beam influenced by the crack, and over which ϕ_2 exists, must be assumed. In applying the conjugate beam method, ϕ_2 is then taken as the unknown, and a solution obtained in terms of experimentally observed deflections.

The moment-curvature relationships computed in this manner are useful in comparing the performance of the test specimens cast with various fibers. Since the effects of crack location and loading are considered, and the section geometry is common for all of the test specimens, differences in behavior can be attributed directly to material properties at the failure section.

3.4.2 EXPERIMENTAL MOMENT-CURVATURE RELATIONSHIPS

For the purposes of this investigation, the region of constant curvature surrounding a crack was assumed to be as wide as the depth of the beam. With this assumption, moment-curvature relationships were determined from test data for eighteen fiber reinforced concrete flexural specimens. It was not possible to determine representative M - ϕ relationships for the remaining thirteen fiber reinforced specimens for several reasons. All specimens with hot melt fibers fractured with no inelastic curvature after crack initiation. In the case of two F1.5 specimens, load carrying capacity dropped to 30 percent of the cracking load immediately after crack initiation. In the remaining cases the crack formed either outside or near the end of the region of measured deflection, and calculation of the M - ϕ relationship was unreliable.

Moment-curvature relationships are plotted for each fiber type in Figs. 3.13 through 3.17. In Figs. 3.18 and 3.19, several of the M - ϕ curves have been repeated to show behavior over a wider range of curvature.

In the 0.9 percent series, except for both specimens with the bent-end fiber, and one specimen with the enlarged-end fiber, the maximum load sustained occurred at cracking of the specimen. For the 1.5 percent series the trend is reversed; except for one R1.5 and both W1.5 specimens, the beams sustained loads higher than the cracking load.

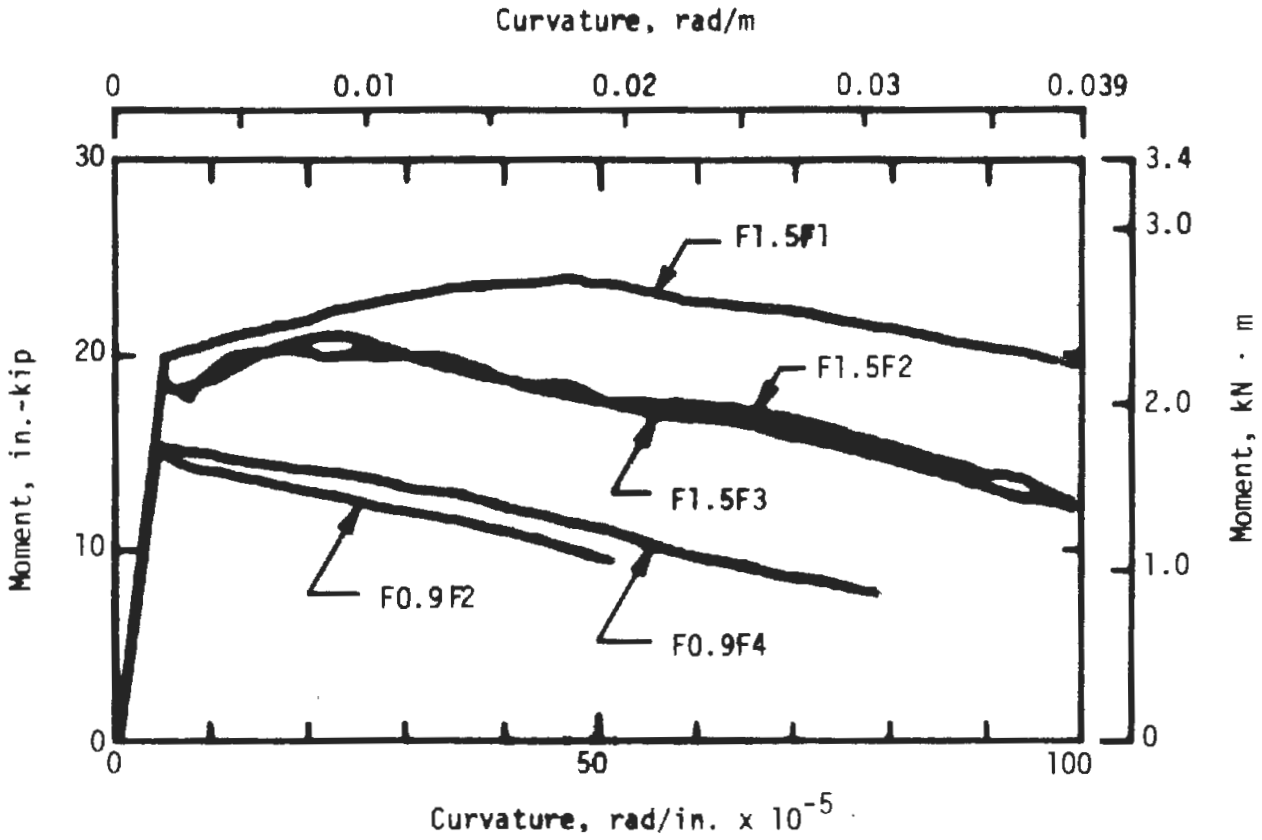

FIG. 3.13 MOMENT-CURVATURE RELATIONSHIPS FOR CONCRETES WITH FLAT FIBERS

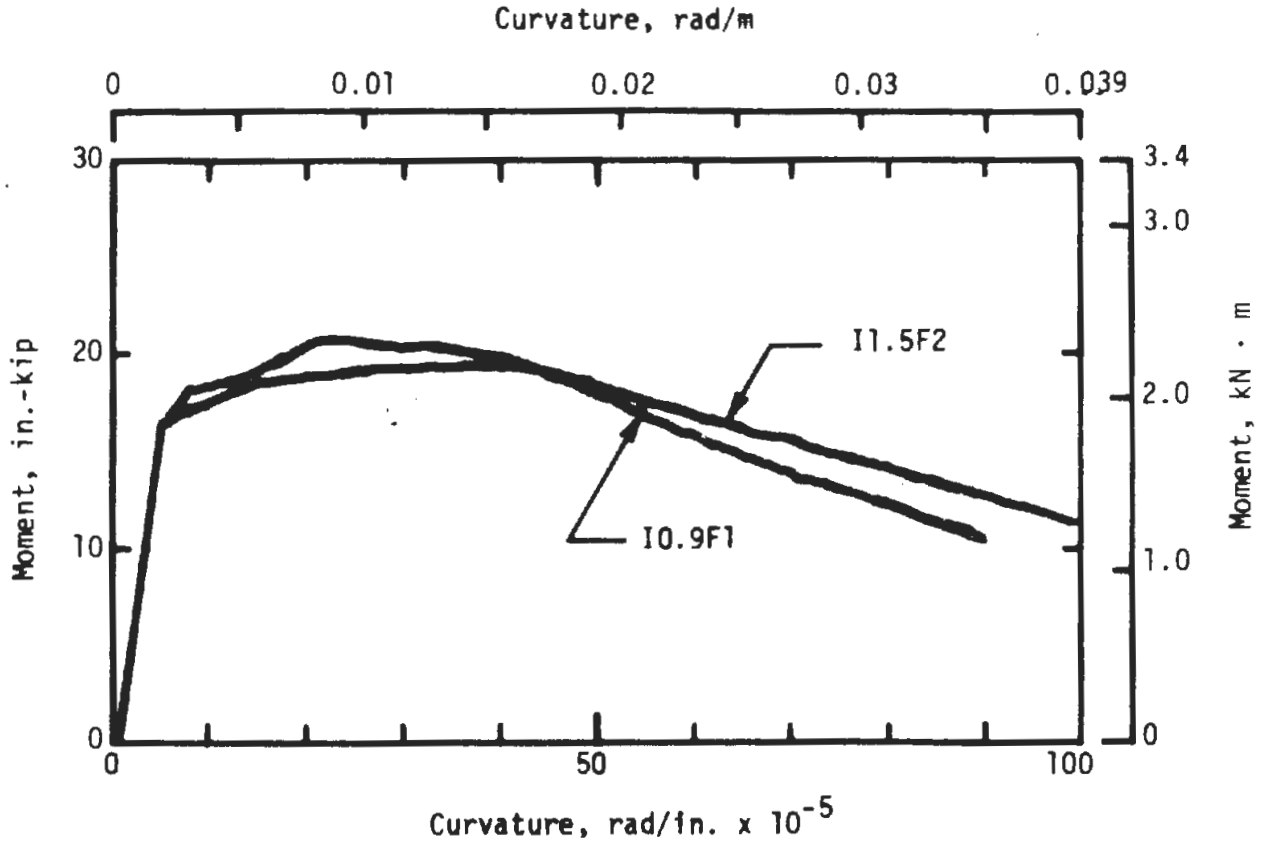

FIG. 3.14 MOMENT-CURVATURE RELATIONSHIPS FOR CONCRETES WITH ENLARGED-END FIBERS

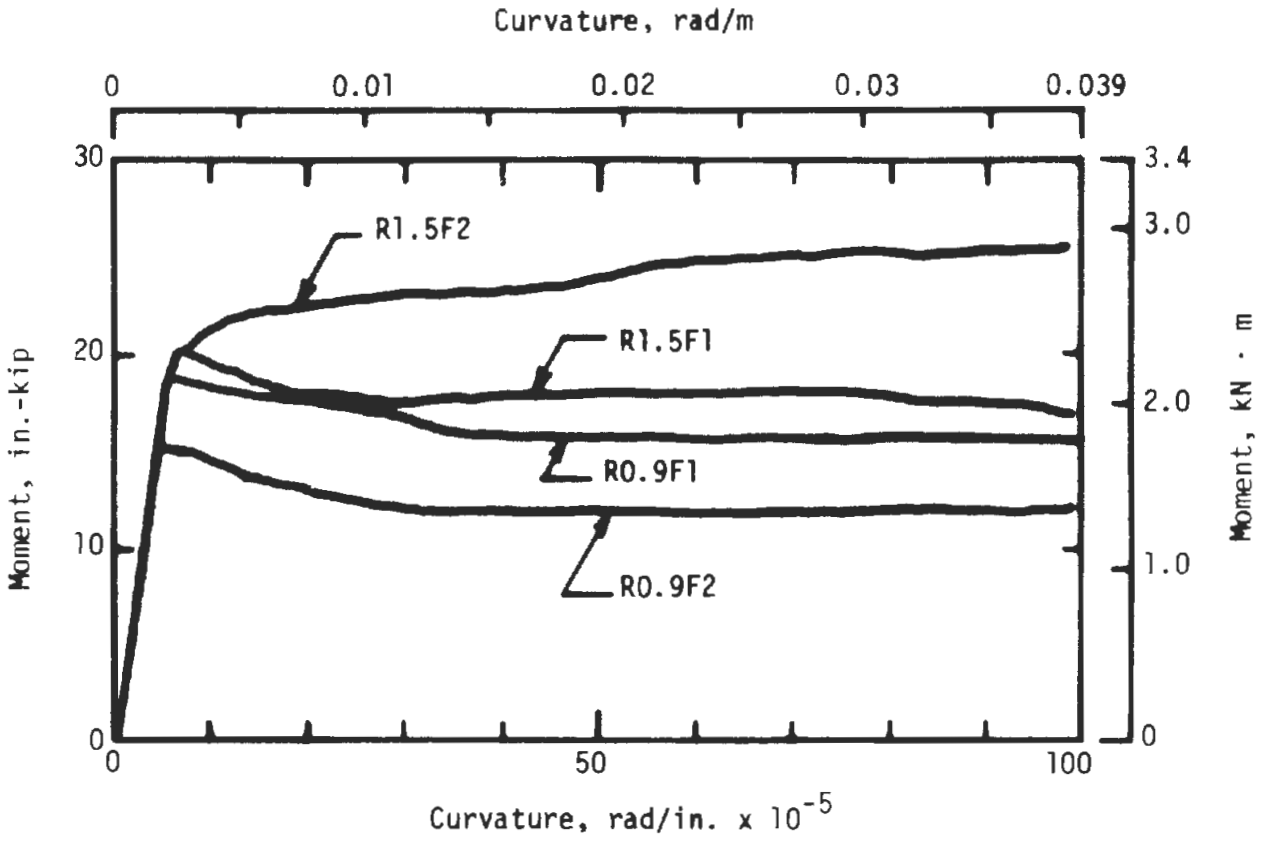

FIG. 3.15 MOMENT-CURVATURE RELATIONSHIPS FOR CONCRETES WITH ROUND FIBERS

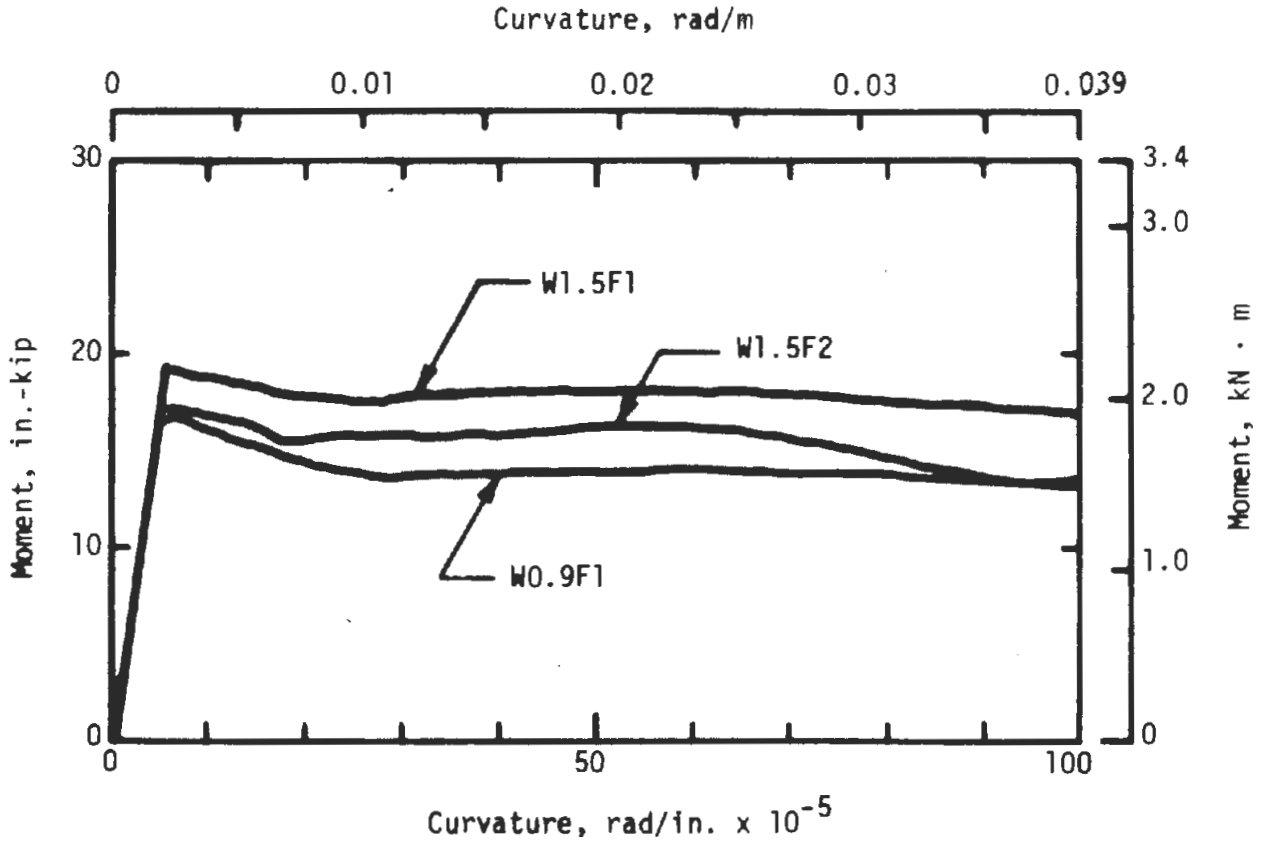

FIG. 3.16 MOMENT-CURVATURE RELATIONSHIPS FOR CONCRETES WITH CRIMPED FIBERS

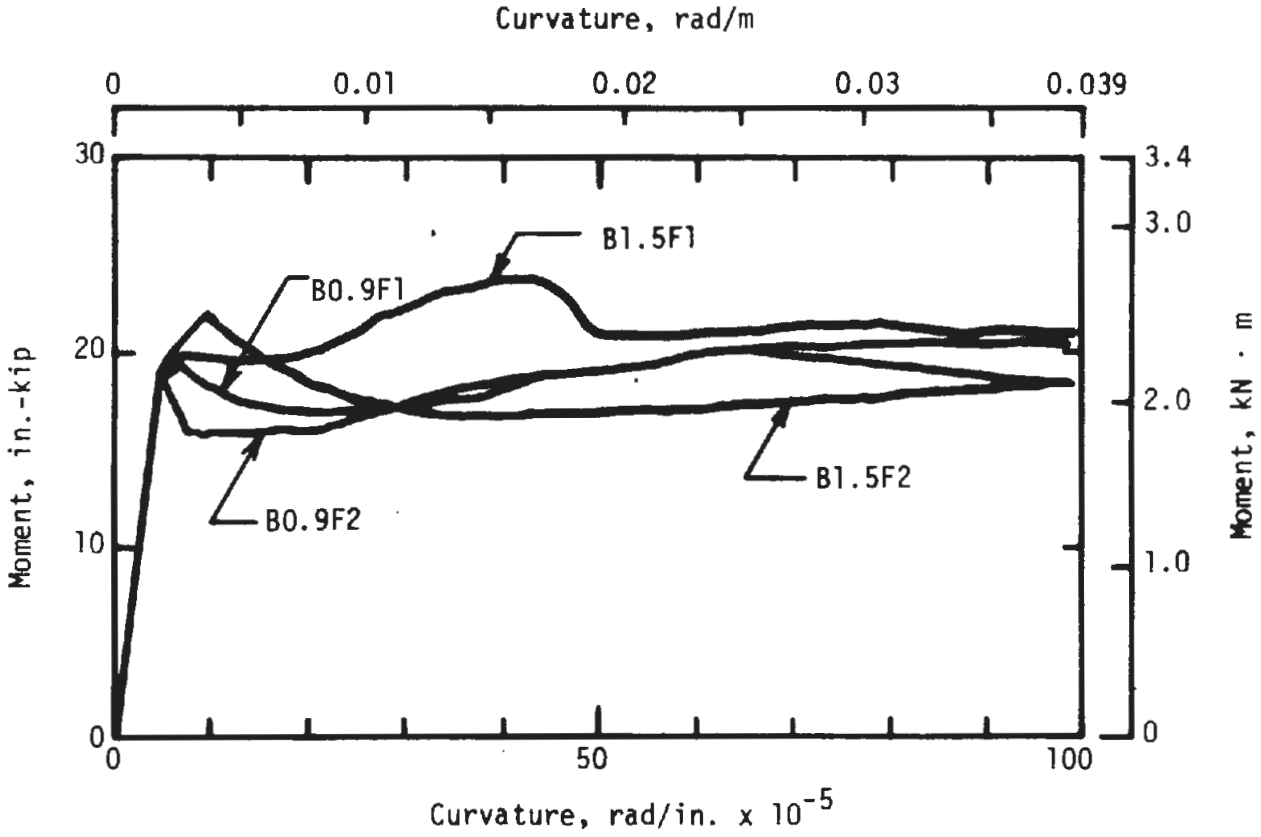

FIG. 3.17 MOMENT-CURVATURE RELATIONSHIPS FOR CONCRETES WITH BENT-END FIBERS

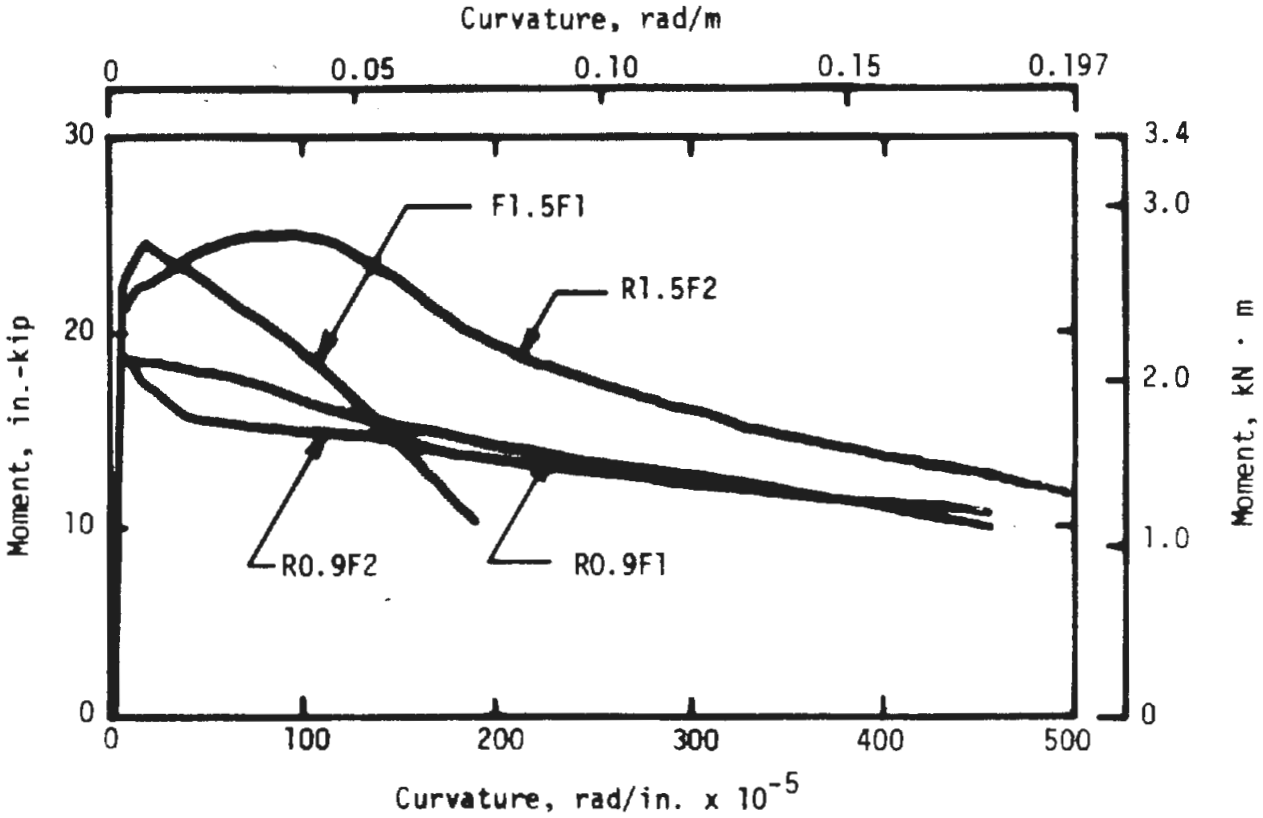

FIG. 3.18 MOMENT-CURVATURE RELATIONSHIPS FOR PLAIN FIBERS

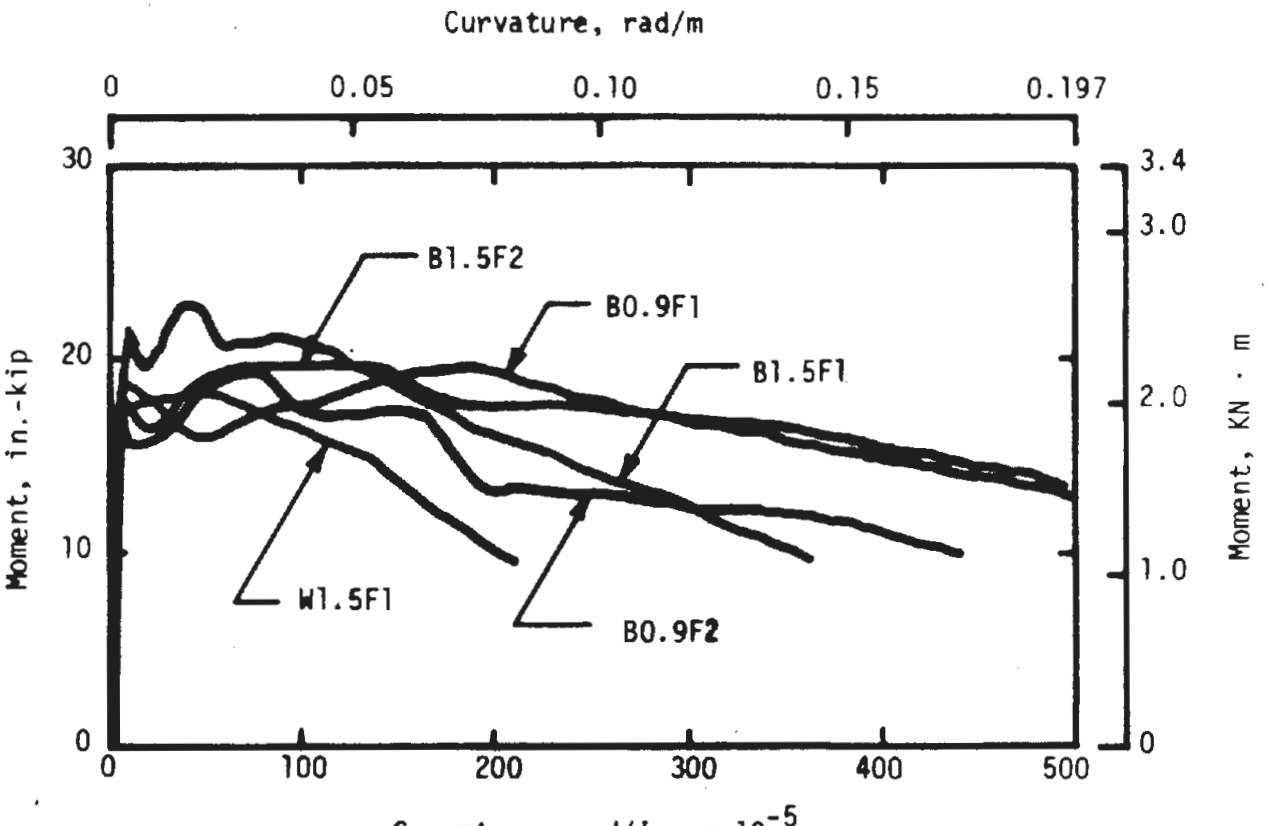

FIG. 3.19 MOMENT-CURVATURE RELATIONSHIPS FOR DEFORMED FIBERS

For each fiber type the character of the descending branch is similar for the 0.9 and 1.5 percent series. The effect of fiber content is manifested in matrix cracking level, an effect related to the cement content required for workability, and in the relative cracking and postcracking strengths. For specimens with higher postcracking strength, the maximum load occurred at a curvature of 4 to 10 times the cracking curvature.

A further observation is pertinent regarding the specimens which sustained loads higher than cracking. In nearly all cases load dropped after cracking, then increased with increased curvature. This behavior can be measured because deformation, rather than load, is applied during testing. Similar behavior is observed in ordinary reinforced concrete members, and can be predicted from geometric and stress-strain properties of the member components. The variability in the experimentally determined M - ϕ relationships, even for the same fiber type and content, underscores the realities of concrete testing. The limited sampling of test specimens available in this study are then useful in establishing trends, but absolute magnitudes should be applied with judgement.

3.5 STRESS-STRAIN RELATIONSHIPS

Using the techniques described in Appendix B, a nominal tensile stress-strain relationship was determined for each of the eighteen beam specimens with suitable moment-curvature relationships. The stress-strain relationships are presented in Figs. 3.20 to 3.29 for each fiber type and content.

The differences in the stress drop at cracking for various fiber types and contents were less dramatic than anticipated. More important

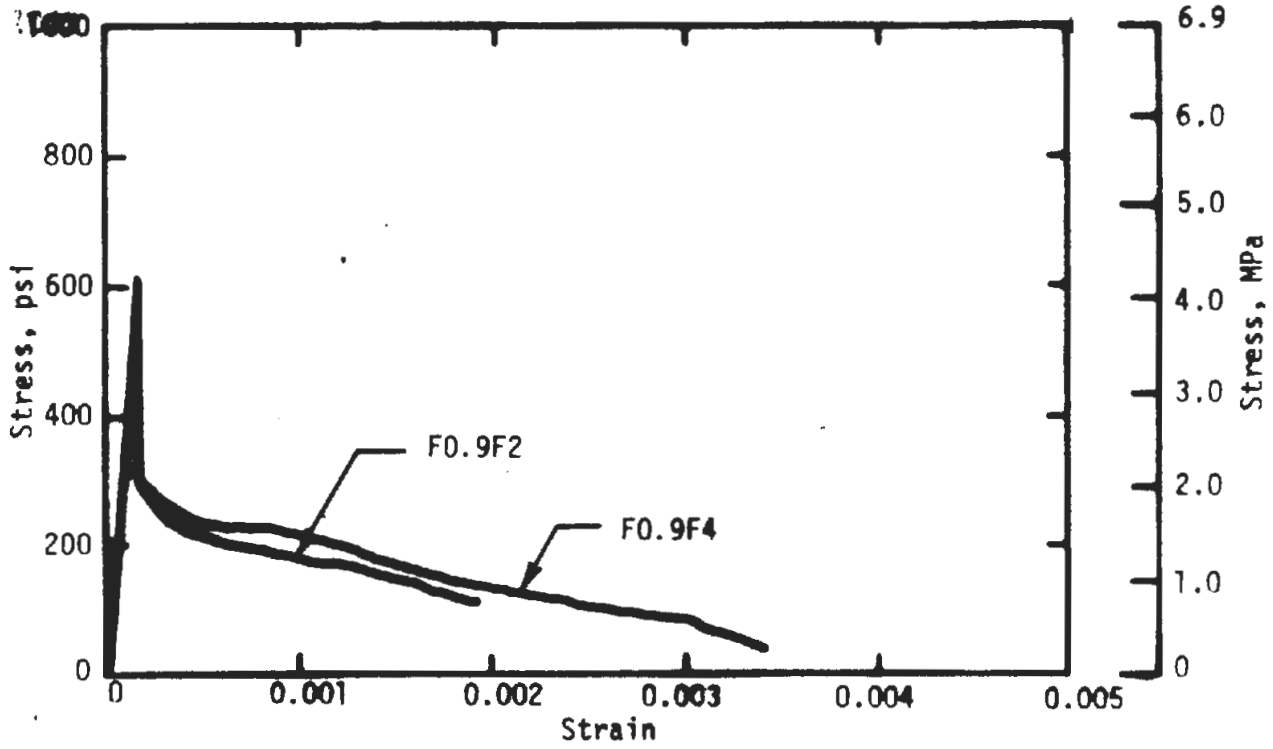

FIG. 3.20 TENSILE STRESS-STRAIN RELATIONSHIPS FOR MIX F0.9

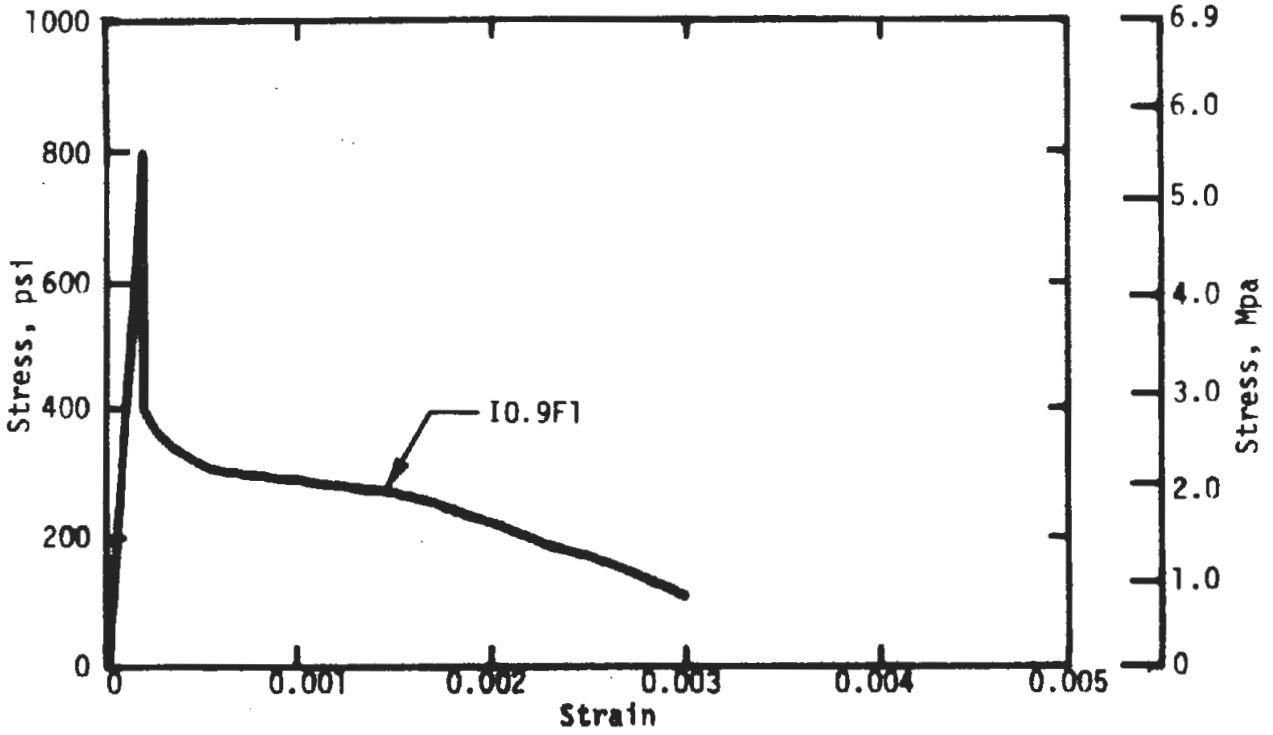

FIG. 3.21 TENSILE STRESS-STRAIN RELATIONSHIP FOR MIX I0.9

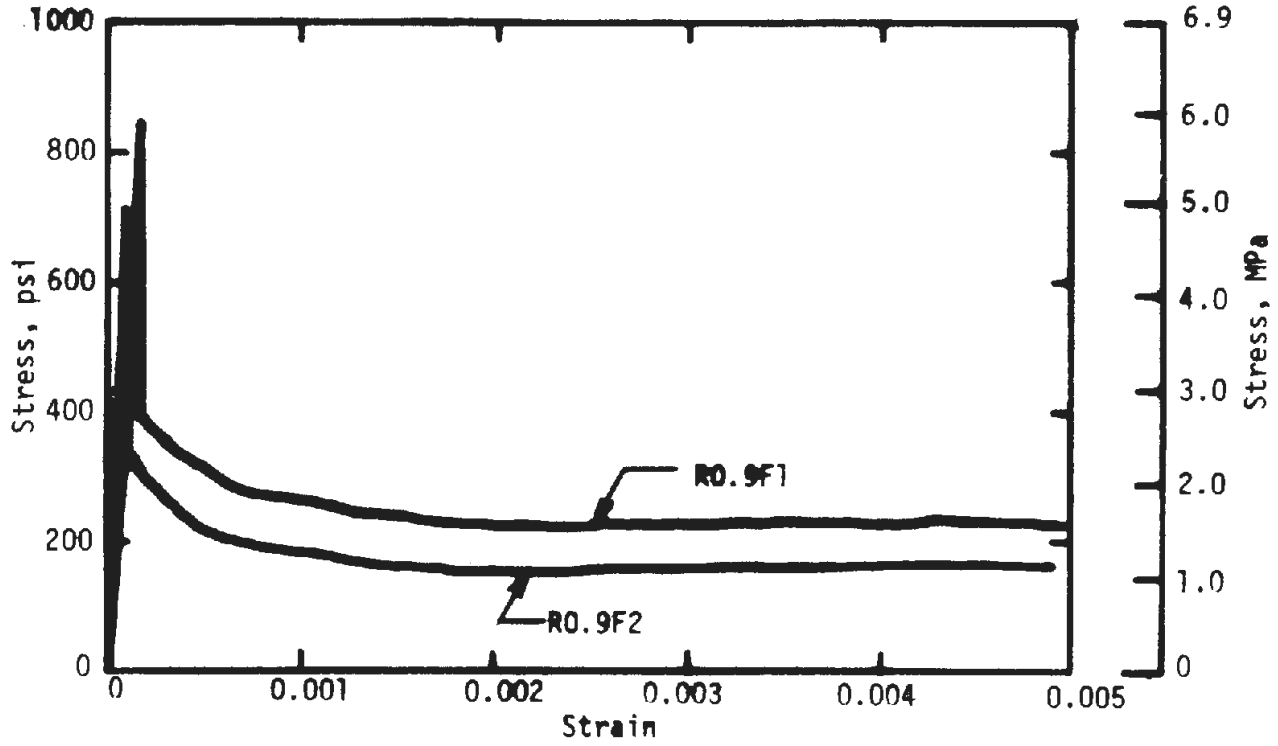

FIG. 3.22 TENSILE STRESS-STRAIN RELATIONSHIPS FOR MIX R0.9

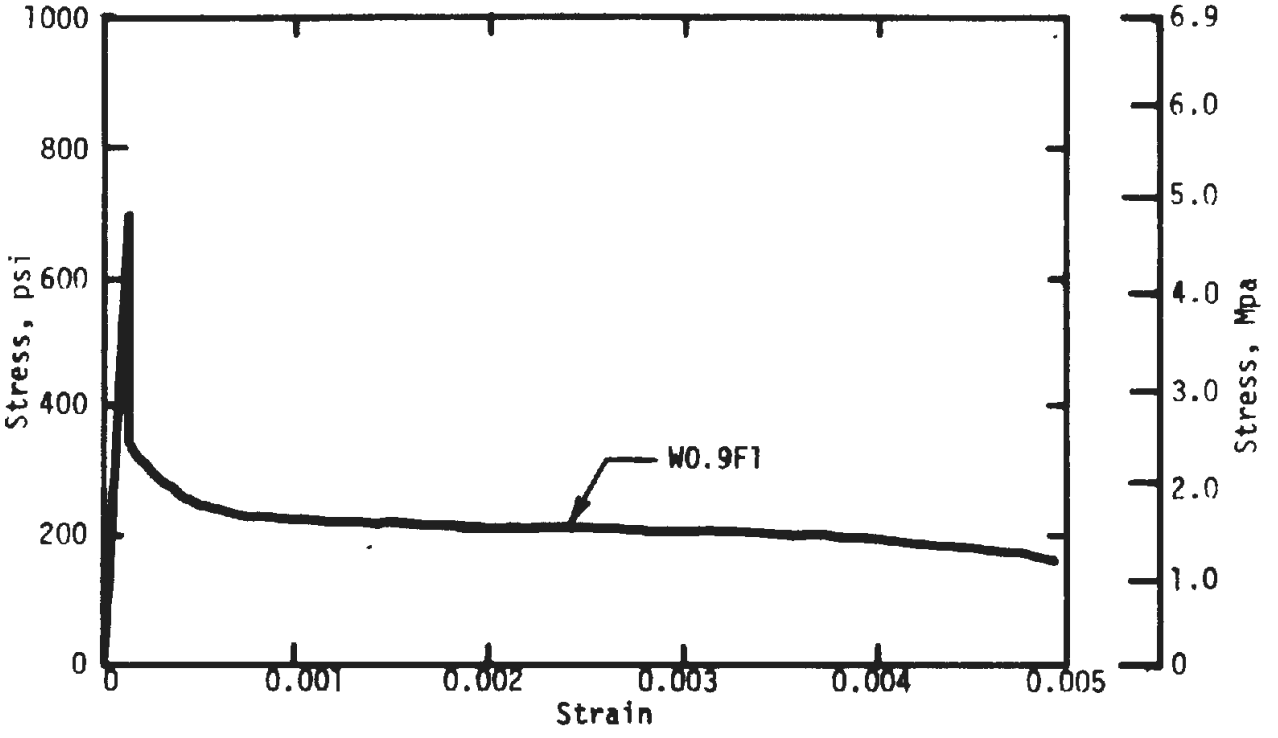

FIG. 3.23 TENSILE STRESS-STRAIN RELATIONSHIP FOR MIX W0.9

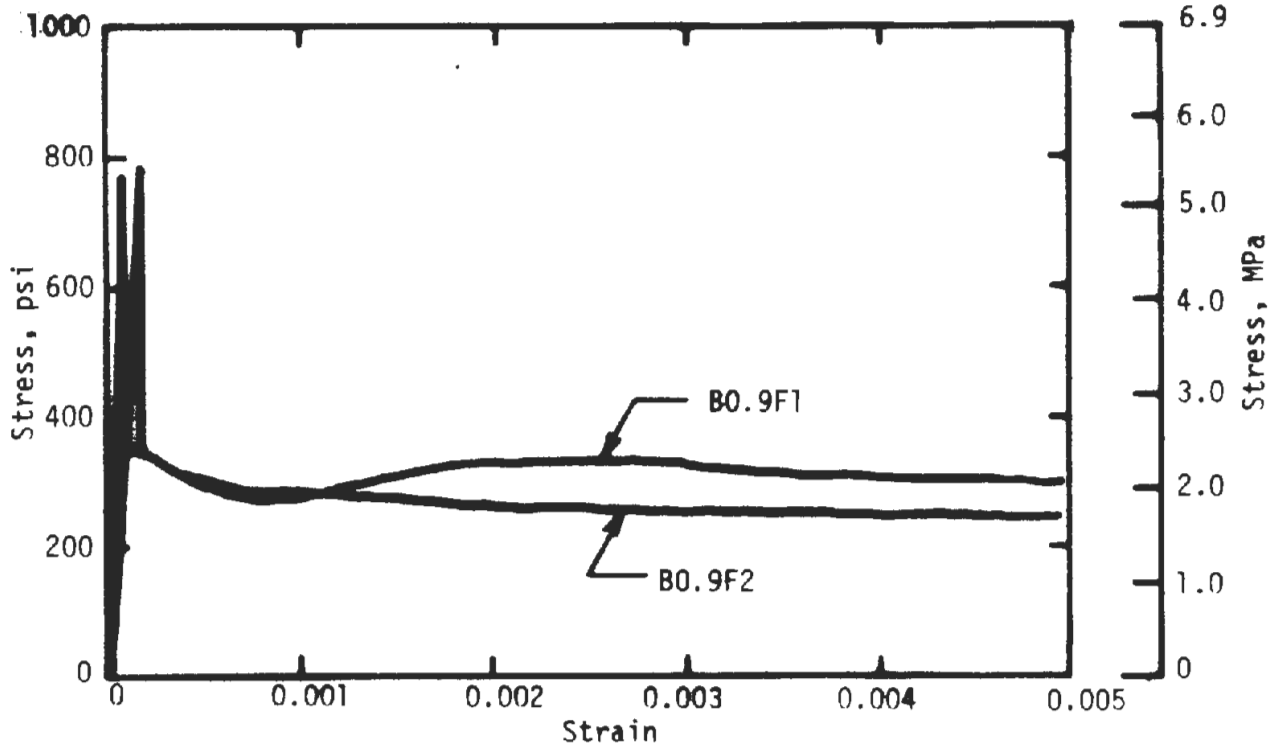

FIG. 3.24 TENSILE STRESS-STRAIN RELATIONSHIPS FOR MIX B0.9

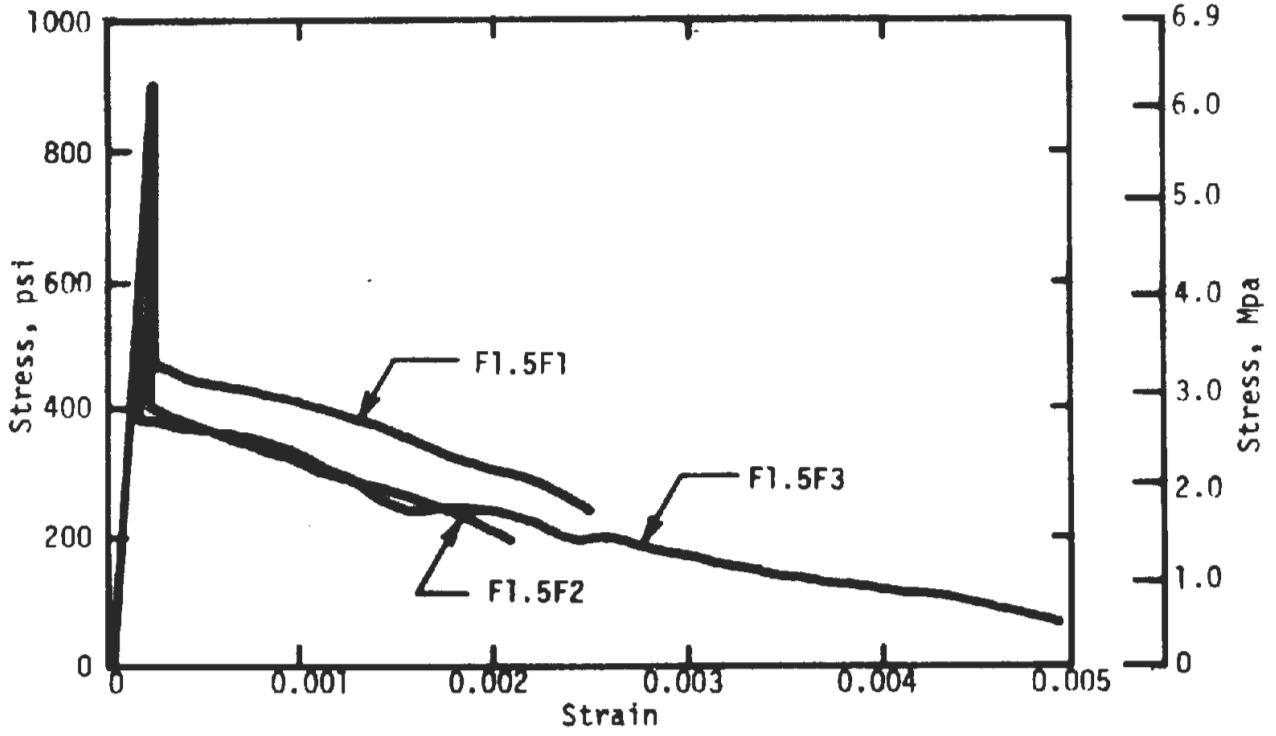

FIG. 3.25 TENSILE STRESS-STRAIN RELATIONSHIPS FOR MIX F1.5

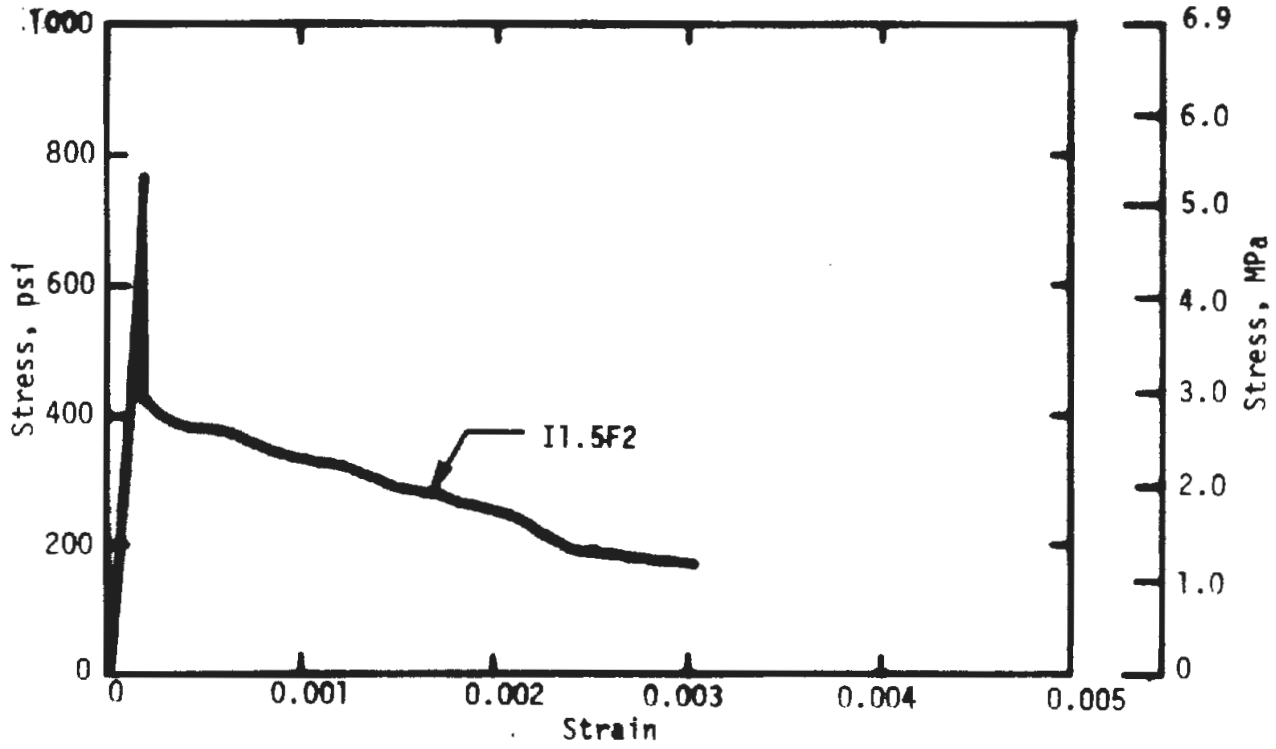

FIG. 3.26 TENSILE STRESS-STRAIN RELATIONSHIP FOR MIX I1.5

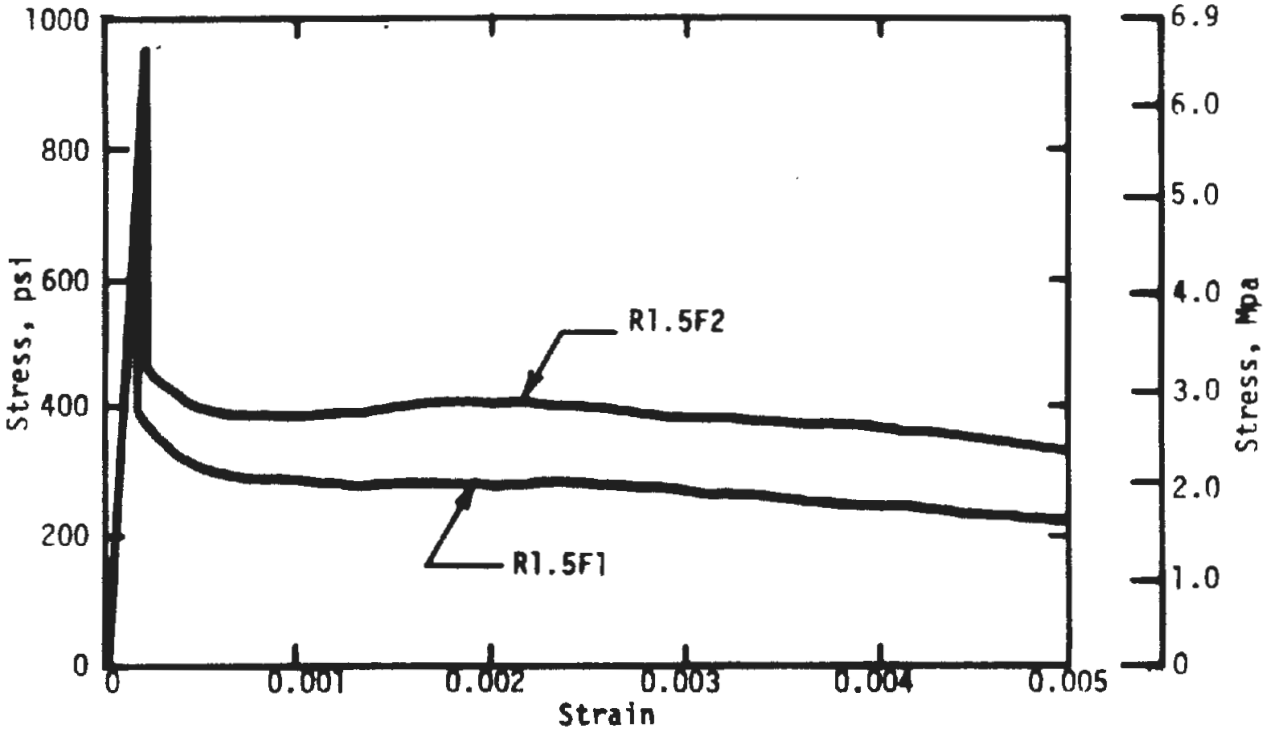

FIG. 3.27 TENSILE STRESS-STRAIN RELATIONSHIPS FOR MIX R1.5

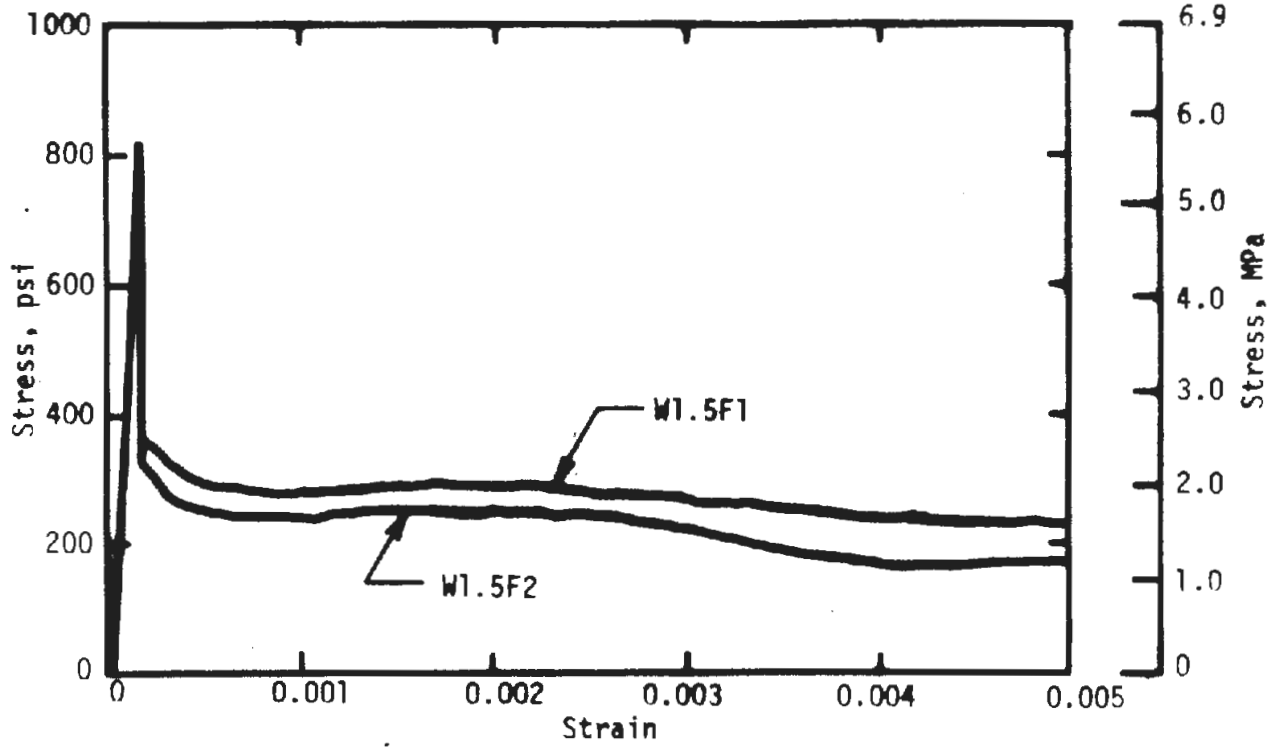

FIG. 3.28 TENSILE STRESS-STRAIN RELATIONSHIPS FOR MIX W1.5

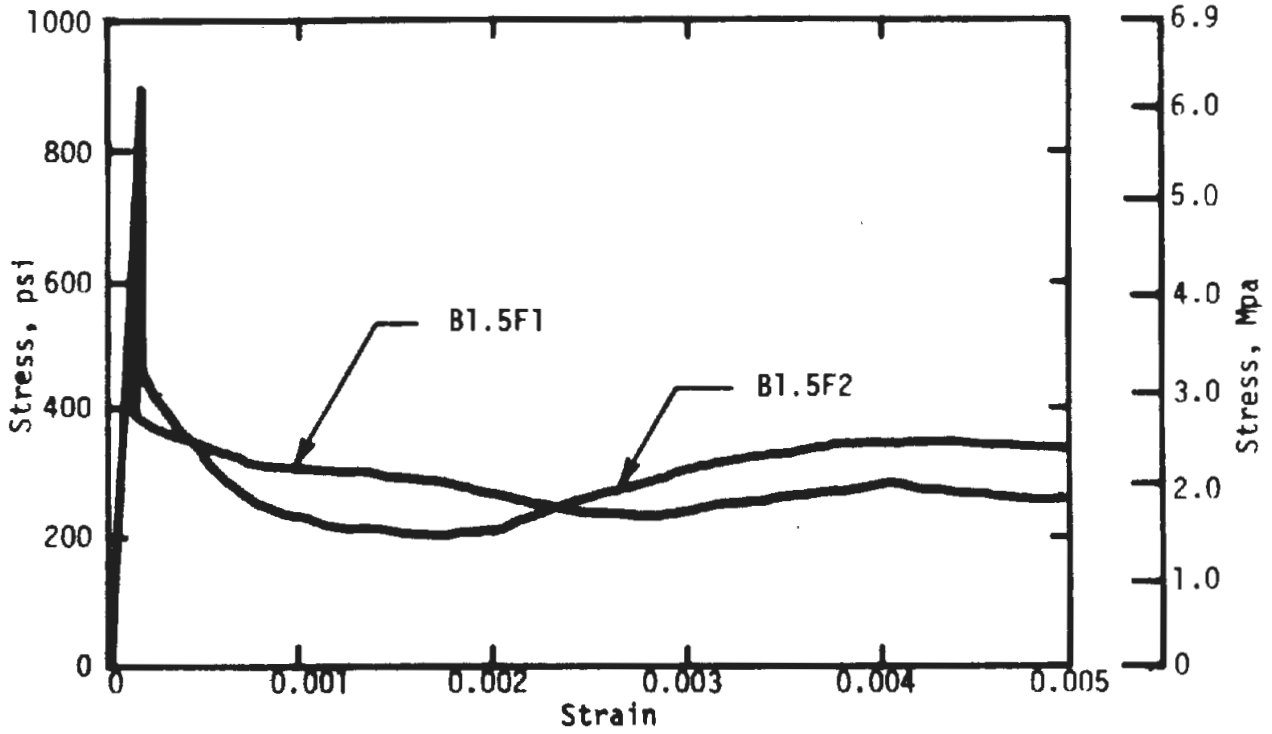

FIG. 3.29 TENSILE STRESS-STRAIN RELATIONSHIPS FOR MIX B1.5

differences are noted in the shape of the stress-strain relationships for the postcracking range. The shapes are similar for all specimens of one fiber type. At both fiber contents the stress-strain relationships for flat and enlarged-end fibers steadily decrease, and do not show a pleateau of constant stress. For the round and crimped fibers there is a further decrease in stress after the drop, but a plateau of constant stress is reached and maintained over a considerable range. For the bent-end fiber the experimentally determined stress-strain relationships differ somewhat from the plateau observed with the round and crimped fibers but the behavior is similar on the whole. Although fiber content does not influence the shape of the computed stress-strain curves, the effect is observed in the level of postcracking stress, and strain at which the stress-strain relationship decays to zero.

The shape of the computed stress-strain relationships are generally consistent with the load-deflection curves obtained from the direct tension tests. Any effects of individual fibers are obscured in the analysis. The high postcracking loads sustained in direct tension by several of the specimens with bent-end fibers are not paralleled in the stress-strain relationships computed from flexural tests. These high loads are probably due to preferential fiber orientation in the region of reduced cross section.

CHAPTER 4

SUMMARY AND CONCLUSIONS

4.1 SUMMARY

This study has compared the performance of fiber reinforced concrete made with six different steel fibers to determine differences in behavior which may be attributed to fiber bond and anchorage characteristics related to physical deformation.

Fiber reinforced concrete mixes were designed for two fiber contents, 0.9 and 1.5 volume percent. Plain concrete mixes were formulated for comparison of strength and stiffness.

A total of forty-three 4 in. by 6 in. by 64-in. (100 mm by 150 mm by 1625-mm) beam specimens were tested to determine flexural load-deflection characteristics. Specimens were cast from each batch to determine compressive strength and modulus of rupture. Direct tension specimens were cast from alternate batches.

Compressive strengths of all the concretes were in the range of 7000-8000 psi (50-55 MPa). The modulus of rupture determined from a 3 in. by 3 in. by 15-in. (75 mm by 75 mm by 380-m) beam was in the range of 900-1700 psi (6-12 MPa). The nominal modulus of rupture determined from the 4 in. by 6 in. by 64-in. (100 mm by 150 mm by 1625-mm) beams was lower than that obtained from the control specimens. The difference averaged 30 percent for the fiber reinforced concrete and 25 percent for plain concrete.

The strengths of mix designs of the 1.5 volume percent fiber content are in nearly all cases higher than at 0.9 volume percent because of the

increased paste content. The difference was about 500 psi (3.5 MPa) in compression, and less than 200 psi (1.4 MPa) in modulus of rupture for the small beams. In some cases, the strengths of the larger beam specimens with fiber reinforcement were lower than the plain concrete control mixes. Nominal strength in direct tension was 600 psi (4.1 MPa), with fiber geometry and content influencing only the postcracking behavior.

The mean strengths obtained in this study are of a necessarily small sample. Variability in the results is dependent on loading conditions, mode of failure, fiber content, and fiber type.

The load-deflection curves for eighteen of the 4 in. by 6 in. by 64-in. (100 mm by 150 mm by 1625-mm) fiber reinforced concrete beams were used to determine moment-curvature and stress-strain relationships for the region surrounding the flexural crack. In the 0.9 percent series, except for both specimens with the bent-end fiber, and one specimen with the enlarged-end fiber, the maximum load sustained occurred at cracking of the specimen. For the 1.5 percent series the trend is reversed. Except for one specimen with the round fiber, and both specimens with the crimped fiber, the beam sustained loads higher than the cracking load. The determination of load-deflection behavior beyond the maximum load was possible since the specimens were tested by applying deformation rather than load. For specimens which sustain post-cracking loads higher than the cracking load, the maximum load occurs at a curvature of 4 to 10 times the cracking curvature. Computed stress-strain relationships show either strain softening behavior immediately after cracking or an extended region of nearly constant stress. The character of the post-cracking region is similar for all specimens of one fiber geometry. Fiber content and geometry determine postcracking stress levels.

With the exception of the performance of the round fiber, the behavior of the various fiber reinforced concretes is consistent with respect to fiber anchorage. The enlarged-end fiber is not very efficient in the postcracking range. These fibers may either pullout or fracture, and it is possible that the pullout mode of this fiber may be less ductile than for the crimped or bent-end fibers. The behavior of the round fibers in the postcracking range cannot be explained on the basis of physical deformation.

4.2 CONCLUSIONS

Steel fiber reinforced concrete cannot be evaluated in terms of strength alone. Postcracking resistance may vary considerably depending on the fiber material and the individual fiber failure mode, as well as fiber content and orientation. To achieve the maximum benefit of fiber reinforcement, it is essential to have a ductile fiber with a ductile failure mode.

Mix designs must be formulated with due regard to the application of the end product. Both loading and structural system must be considered. In a highly redundant system, such as a slab on grade, the system can withstand considerable redistribution of moments and the descending branch of the moment-curvature relationship becomes important. In contrast, no moment redistribution can occur for a simply supported beam.

Further studies would be valuable in establishing criteria for predicting the behavior of a system on the basis of mix design and member geometry. This study has indicated that, for ductile straight fibers, the maximum postcracking load can exceed the cracking load at several times the cracking deflection if the quantity $\rho\frac{\ell}{d}$ is greater than 90, where ρ is the

fiber content by volume expressed in percent, and $\frac{\ell}{d}$ is the fiber aspect ratio. For anchored fibers the critical value is less than 90, but the exact value is uncertain. The critical value of $\rho\frac{\ell}{d}$ may additionally be a function of concrete matrix strength, relative size of fiber and member, and fiber orientation.

The utilization of properly anchored fiber reinforcement may allow reduced paste and fiber contents while keeping properties constant. Alternately, an overall improvement in the properties of the hardened concrete may be obtained at constant fiber content. Further study of the behavior of concrete reinforced with anchored fibers will contribute to the technology available for the appropriate design and control of all fiber reinforced concrete.

APPENDIX A

PULLOUT LOADS

A.1 INTRODUCTION

Pullout loads of individual fibers can be evaluated by means of simple and direct procedures. The purpose of this Appendix is to present data which supplements the present investigation, but was not directly related.

A.2 PROCEDURE

Fibers were cast in a matrix of fiber reinforced concrete. Embedment lengths of 0.25, 0.50 and 0.75 in. (6.3, 12.7 and 19.1 mm) were studied for each fiber type. Tests were made at 7 and 28 d.

The test apparatus consisted of a can attached to a drill chuck. The chuck was clamped onto the fiber and fine sand slowly poured into the can. After pullout, the total weight of the can and sand chuck were recorded as the pullout load.

A.3 RESULTS AND DISCUSSION

Pullout loads are reported in Table A.1 for the six fiber geometries considered in this investigation. Inconsistencies in pullout load are apparent with respect to both test age and embedment length. This is especially evident for fibers I and B, those with deformation in the end region. The limited results included in Table A.1 indicate that a large population of data is required to fully appreciate pullout behavior of single fibers. The results are of use in general comparison of various fiber geometries.

LIST OF REFERENCES

1. ACI Committee 544, "State of The Art Report on Fiber Reinforced Concrete," ACI Journal, November 1973, Title 70-65.

2. American Society for Testing and Materials, 1975 Annual Book of ASTM Standards, Philadelphia, 1975.

3. Batson, G., E. Jenkins and R. Spatney, "Steel Fibers As Shear Reinforcement in Beams," ACI Journal, October 1972, Title 69-61.

4. Burnett, E.F.P., T. Constable and P. Cover, "Centrifugated Wire Fiber Reinforced Concrete," ACI Special Publication, SP 44-26, 1974.

5. Dehousse, N. M. and A. LeJeune, "Les Mortiers Et Betons Reinforces De Fibres Metalliques," Conference on Properties and Applications of Fiber Reinforced Concrete and Other Fiber Reinforced Building Materials, Stevin Laboratory, Delft, The Netherlands, 1973.

6. Edgington, J., D. J. Hannant and R.I.T. Williams, "Steel Fibre Reinforced Concrete," Building Research Establishment Current Paper 69/74, Building Research Station, Garston Watford, U.K., 1974.

7. Henry, R.L., "An Investigation of Large Diameter Fiber Reinforced Concrete Pipe," ACI Special Publication, SP 44-25, 1974.

8. Herring, K.S., J. W. Laws, C. E. Kesler, S. L. Paul and A. R. Robinson, "Concrete for Tunnel Liners: Behavior of Steel Fiber Reinforced Concrete Under Combined Loads," Report No. FRA-ORDD 75-7, 1975. (NTIS PB 237 382/AS)

9. Johnston, C.D., "Steel Fiber Reinforced Mortar and Concrete: A Review of Mechanical Properties," ACI Special Publication, SP 44-7, 1974.

10. Johnston, C.D. and R. A. Coleman, "Strength and Deformation of Steel Fiber Reinforced Mortar in Uniaxial Tension," ACI Special Publication, SP 44-10, 1974.

11. Kesler, C. E., "Mix Design Considerations," Conference Proceedings M-28, Fibrous Concrete - Construction Material for the Seventies, U.S. Army Construction Engineering Research Laboratory (CERL), Champaign, Illinois, December 1972, pp. 27-37.

12. Kesler, C. E., Private Communication, 1975.

13. Luke, C. E., B. L. Waterhouse and J. F. Wooldridge, "Steel Fiber Reinforced Concrete Optimization and Applications," ACI Special Publication, SP 44-23, 1974.

14. Moens, J., "Steel Wire Fiber Optimization," Conference on Properties and Applications of Fiber Reinforced Concrete and Other Fiber Reinforced Building Materials, Stevin Laboratory, Delft, The Netherlands, 1973.

15. Ounanian, D.W., G. T. Halvorsen and C. E. Kesler, "Concrete for Tunnel Liners: Pumpable Fiber Reinforced Concrete," Report No. FRA-OR&D-75-88. (NTIS PB 248 636/AS)

16. Patent No. 3,592,720. To National-Standard Company, Niles, Michigan. U.S. Patent Office, Washington, D.C.

17. Paul, S.L. and R. A. Ferrera-Boza, "Concrete Tunnel Liners: Structural Testing of Cast-In-Place Liners," Report No. FRA-OR&D 75-94. (NTIS PB 252 935/AS)

18. Tattersall, G. H. and C. R. Urbanowicz, "Bond Strength in Steel-Fibre-Reinforced Concrete," Magazine of Concrete Research, Vol. 26, No. 87, June 1974.

19. Taylor, M.A., "Closed Loop Fiber Reinforcement for Concrete," ACI Special Publication, SP 44-17, 1974.

TABLE A.1

SINGLE FIBER PULLOUT LOADS

Fiber	Pullout load, lbf (N)[1]					
	Embedment length, in. (mm), 7-d test			Embedment length, in. (mm), 28-d test		
	0.25 (6.3)	0.50 (12.7)	0.75 (19.1)	0.25 (6.3)	0.50 (12.7)	0.75 (19.1)
F	1.70 (7.56)	5.99 (26.64)	10.73 (47.73)	10.60 (47.15)	14.93 (66.41)	16.67 (74.15)
I	17.80 (79.18)	12.51 (55.65)	19.49 (86.70)	23.15 (102.98)	24.55 (109.20)	20.64 (91.81)
H	12.34 (54.89)	19.80 (88.07)	20.77 (92.39)	21.32 (94.84)	24.19 (107.60)	28.14 (125.17)
R	1.82 (8.10)	2.80 (12.46)	5.31 (23.62)	5.76 (25.62)	11.31 (50.31)	16.12 (71.71)
W	13.97 (62.14)	21.50 (95.64)	21.88 (97.33)	17.18 (76.42)	20.48 (91.10)	21.74 (96.70)
B	12.51 (55.65)	12.99 (57.78)	15.27 (67.92)	20.98 (93.32)	23.23 (103.33)	19.25 (85.63)

[1] After Kesler [12]

APPENDIX B

ANALYTICAL DETERMINATION OF TENSILE STRESS-STRAIN RELATIONSHIP FROM BEAM TESTS

B.1 SCOPE

The purpose of this Appendix is to briefly summarize the analytical techniques used to determine the tensile stress-strain relationship from beam tests. These techniques have been utilized at the University of Illinois since 1973, and have been described in detail by Herring, et al., [8].

By adopting an engineering approach to observed behavior a model is developed on the macro level, without considering concepts such as crack arrest, fiber pullout, or the mechanics of composite materials. This model may then be used to predict behavior in a variety of situations.

B.2 MODEL OF STRESS-STRAIN BEHAVIOR

Observed flexural load-deflection behavior for fiber reinforced concrete includes an initial region which is essentially linear. At some point there is a noticeable discontinuity in the slope of the load-deflection and corresponding moment-curvature relationships. This discontinuity of slope is assumed to correspond to the initiation of cracking at the macroscopic level.

The slope discontinuity of the M - ϕ relationship requires a discontinuity in the stress-strain relationship at the point of cracking. From consideration of equilibrium of the section just after cracking it can be shown that

$$\Delta\sigma = \frac{2\,\sigma_o\,\Delta M'}{3EI - \Delta M'}$$

where

$\Delta\sigma$ = the magnitude of the stress drop,

σ_o = the stress at cracking computed from linear theory,

$\Delta M'$ = the change in slope of the M - ϕ relationship at cracking, and

EI = the elastic stiffness of the section.

Since $\Delta\sigma$ is a stress drop, $\Delta M'$ must be negative.

After the stress drop, the character of the stress-strain relationship is related to fiber orientation and anchorage. At this time the behavior after the stress discontinuity must be determined empirically, although prediction of this behavior may be possible.

B.3 ANALYTICAL DETERMINATION OF THE STRESS-STRAIN RELATIONSHIP IN TENSION

To determine the tension stress-strain relationship from the results of flexural tests, care must be exercised throughout the experimental and analytical procedures. Once the load-deflection history of the specimen is digitized, either by using electronic data handling techniques or by selecting points from x-y plots obtained during testing, the problem is entirely computational. The computational efforts are divided between determination of the stress drop, and determination of the behavior beyond the stress drop.

Experience of Herring, et al., [8], Paul and Ferrera-Boza [17], and the present investigation have indicated that the optimum procedure for computing the stress-strain relationship beyond the stress discontinuity includes a smoothing of the moment-curvature relationship by fitting a polynomial of high order to the test data.

By evaluating the slope of the best-fit curve at the point of cracking, the stress drop is obtained directly and more sophisticated procedures are not required. Beyond the stress drop, each additional point of the stress-strain relationship is numerically determined by imposing strain compatibility, equilibrium of the cross section, and using the portion of the stress-strain relationship already determined. A Newton-Raphson procedure is employed in iterating to determine the stress corresponding to successive values of strain. The numerical procedures are stable if the moment-curvature relationship is reasonably smooth. In this investigation polynomials of degree 25 to 30 were used successfully.